2018-07-01

Image Source Modeling of Time Reversal for Room Acoustics Applications

Michael Hunter Denison
Brigham Young University

Image Source Modeling of Time Reversal for Room Acoustics Applications

Michael Hunter Denison

A thesis submitted to the faculty of
Brigham Young University
in partial fulfillment of the requirements for the degree of

Master of Science

Brian E. Anderson, Chair
Tracianne B. Neilsen
Kent L. Gee

Department of Physics and Astronomy

Brigham Young University

ABSTRACT

Image Source Modeling of Time Reversal for Room Acoustics Applications

Michael Hunter Denison
Department of Physics and Astronomy, BYU
Master of Science

Time Reversal (TR) is a technique that may be used to focus an acoustic signal at a particular point in space. While many variables contribute to the quality of TR focusing of sound in a particular room, the most important have been shown to be the number of sound sources, signal bandwidth and absorption properties of the medium [Ribay *et al.*, J. Acoust. Soc. Am. **117**(5), 2866-2872 (2005)]. However, the effect of room size on TR focusing has not been explored. Using the image source method algorithm proposed by Allen and Berkley [J. Allen and D. A. Berkley, J. Acoust. Soc. Am. **65**(4), 943-950 (1979)], TR focusing was simulated in a variety of rooms with different absorption and volume properties. Experiments are also conducted in a couple rooms to verify the simulations. The maximum focal amplitude, the temporal focus quality, and the spatial focus clarity are defined and calculated for each simulation. The results are used to determine the effects of absorption and room volume on TR. Less absorption increases the amplitude of the focusing and spatial clarity while decreasing temporal quality. Dissimilarly, larger volumes decrease focal amplitude and spatial clarity while increasing temporal quality. This thesis also explores the placement of individual transducers within a room. It also compares the layout of several source transducers used for a reciprocal time reversal process. Maximum focal amplitude and spatial clarity are found to increase when the focus location is dual coplanar to the source location while temporal quality is found to decrease in comparison to the case when source and focal location share only one plane. Maximum focal amplitude is found to be at a minimum when the focus location is at the critical distance and increases closer and farther away from the source, while temporal quality steadily decreases and spatial clarity steadily increases farther from the source. The maximum focal amplitude and the temporal quality are not greatly affected by the type of array layout, but a circular array is ideal for maximizing spatial clarity.

Keywords: time reversal, image source method, room acoustics

ACKNOWLEDGMENTS

I would like to acknowledge my appreciation to Dr. Brian Anderson for his support and guidance on this project. His available and approachable advisory style allowed for a constant learning experience and a continually progressive project. I am also grateful for my committee members, Dr. Tracianne Neilsen, and Dr. Kent Gee. A special thanks goes to my peers Sarah Young, Travis Hoyt, Brian Patchett, and Matthew Willardson for their willingness to answer questions and assist in experiments. I give thanks to the BYU Department of Physics and Astronomy and the College of Physical and Mathematical Sciences for providing funding for this project. I especially would like to thank Nan Ah You and Shelena Shamo for their efforts in creating a more socially open graduate student body. Most of all, I would like to thank my lovely wife for her love and support during the busy years of graduate school.

Contents

List of Tables

List of Figures

Chapter 1

Introduction

Private communications, from whispers to encrypted messages, have always played a key role in the success of military operations, business endeavors, and social interactions. The key to the delivery of private communications is that only the sender and the receiver know the secret message. Whispering requires proximity between the sender and the receiver while encrypted messages require that both sender and receiver know a certain code. Neither technique works in a situation where one wants to send a private, audible message across a room to someone who is not prepared with a decrypting code (i.e., has no specialized equipment). Ideally, one could convey this message by focusing the acoustic message to one point in the room and have the message be unintelligible elsewhere. Beamforming techniques with a transducer array could be used to direct sound towards the intended target, but this would make it possible for the signal to be intercepted along its path and a direct line of sight would be needed. Time reversal (TR) achieves focusing of sound by exploiting reflections (reverberation) within the room from many directions, making the signal impossible to directly intercept between the source and the intended target. The signal

observed at locations other than the focusing location would contain multiple copies of the message staggered in time that incoherently sum together. This allows the private message to be intelligible at the intended receiver location and unintelligible elsewhere without specialized processing.

Originally developed for reproducible acoustic signal transmissions in the ocean,[1,2] TR is a process used for focusing sound energy at a particular point in space.[3,4] TR can be used in a variety of applications. In addition to sending private messages, TR has been used to create a high-energy focus for ultrasound medical operations (i.e., lithotripsy),[5] reconstruct source events (e.g., earthquakes),[6] optimize communications in reverberant environments,[7,8,9] and perform nondestructive evaluation of materials.[10,11]

1.1 Ripples in a Pond

A common thought experiment used to illustrate TR involves imagining a pebble being dropped into a pond.[4] As seen in Fig. 1.1, the pebble excites outward traveling ripples on the water's surface. If a video was recorded of the traveling ripples, the video could be watched in reverse. The reversed ripples would converge towards the location where the pebble hit the water's surface.

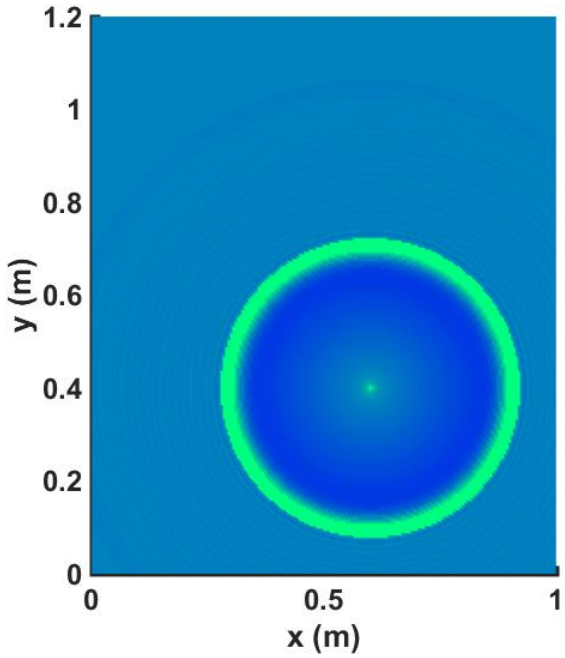

FIG. 1.1. A simulated ripple in water.

The converging ripples could be practically realized by placing a number of transducers, designed to both detect and produce surface waves, on the pond surface. After the pebble is dropped, these transducers would synchronously record waveforms representing the height of the water as a function of time (i.e., the ripples). The recordings could then be time reversed and broadcast from each transducer. Since the recordings made by the transducers would be time-aligned, the broadcasted signals would create converging wave fronts that coalesce at the location where the pebble was dropped. If sufficient transducers are used, these converging wave fronts would reconstruct the ripples observed when the pebble was dropped, only moving in the opposite direction. At the point where the pebble was dropped, the converging ripples would coherently add up their amplitudes and result in a high-amplitude focus location.

Figure 1.2 shows a simulation realizing the ripple thought experiment with six transducers. Figure 1.2(a) shows the ripple diverging from the excitation location at (0.6, 0.4) m, denoted by a filled square. The six transducers, denoted by filled circles, record the ripple response at their locations. The ripple responses are then time reversed and simultaneously broadcast from the respective transducers, as seen in Fig 1.2(b). Figure 1.2(c) shows the wave fronts from each transducer coalescing at the filled square, the original excitation location.

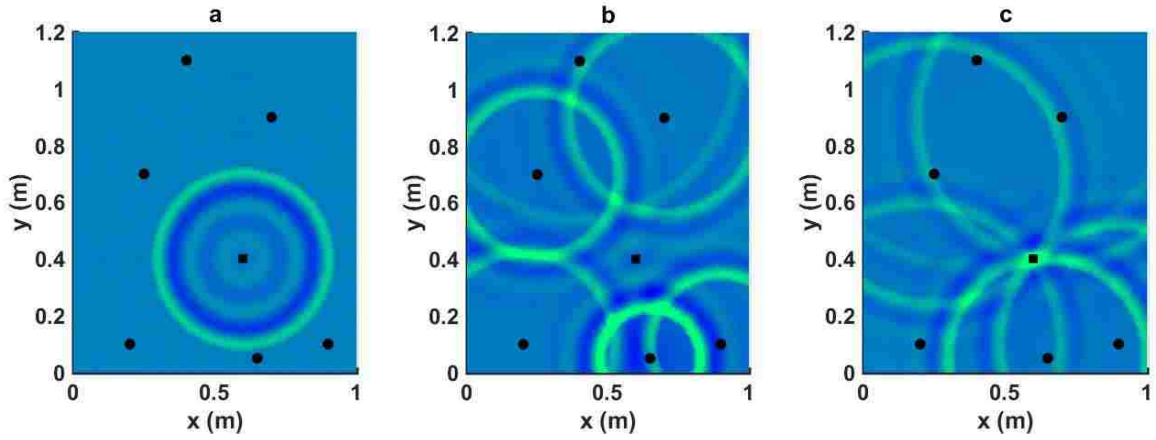

FIG. 1.2. (a) Ripples created by an excitation at (0.6, 0.4) m, denoted by a filled square and transducer locations, denoted by filled circle. (b) Each transducer transmitting their time reversed ripple recorded response. (c) The transmitted signals coalescing to the original excitation location.

In a free-field environment, TR is much like basic beamforming in that it simply time aligns the outputs of each transducer so that the direct sounds arrive at the focus location at the same point in time.[3,12] In an enclosed, or reverberant environment, the TR process also time aligns reflected energy. In an enclosed field, TR is able to focus wave energy with a single source,[13] while beamforming requires multiple sources.

1.2 Time Reversal Fundamentals

A depiction of how standard TR works is shown in Fig. 1.3. It begins with what is known as the forward step, which involves finding the impulse response, $h_{AB}(t)$, between the source at location A and transducer at location B. Experimentally, this is often done by broadcasting a chirp signal from the source and recording the chirp response with the transducer. The cross correlation between the chirp and the chirp response can be used to approximate $h_{AB}(t)$.[14] For simplicity, Fig. 1.3 shows an impulse, $\delta(t)$, being broadcast from a loudspeaker and a microphone recording of $h_{AB}(t)$. The sound travels in every direction from the loudspeaker and follows a very large number of paths between the loudspeaker and microphone. Figure 1.3 shows three recorded paths: the direct sound, a ray of sound with one reflection and a ray of sound with two reflections. When $\delta(t)$ is broadcast from the loudspeaker, the ray that travels the direct path arrives at the microphone first, creating the first arrival in $h_{AB}(t)$. Rays of sound that travel longer paths contribute to later arrivals in $h_{AB}(t)$. $h_{AB}(t)$ contains the amplitude and time of arrival of each ray of sound.

The backward step starts by time reversing $h_{AB}(t)$ to create the time reversed impulse response, $h_{AB}(-t)$ and is broadcast from location B, where the original receiver was located. The sound that traveled the longest path is broadcast first and the sound that traveled the direct path is broadcast last. Each ray of sound retraces its original path and arrives simultaneously at location A, the original broadcast location.

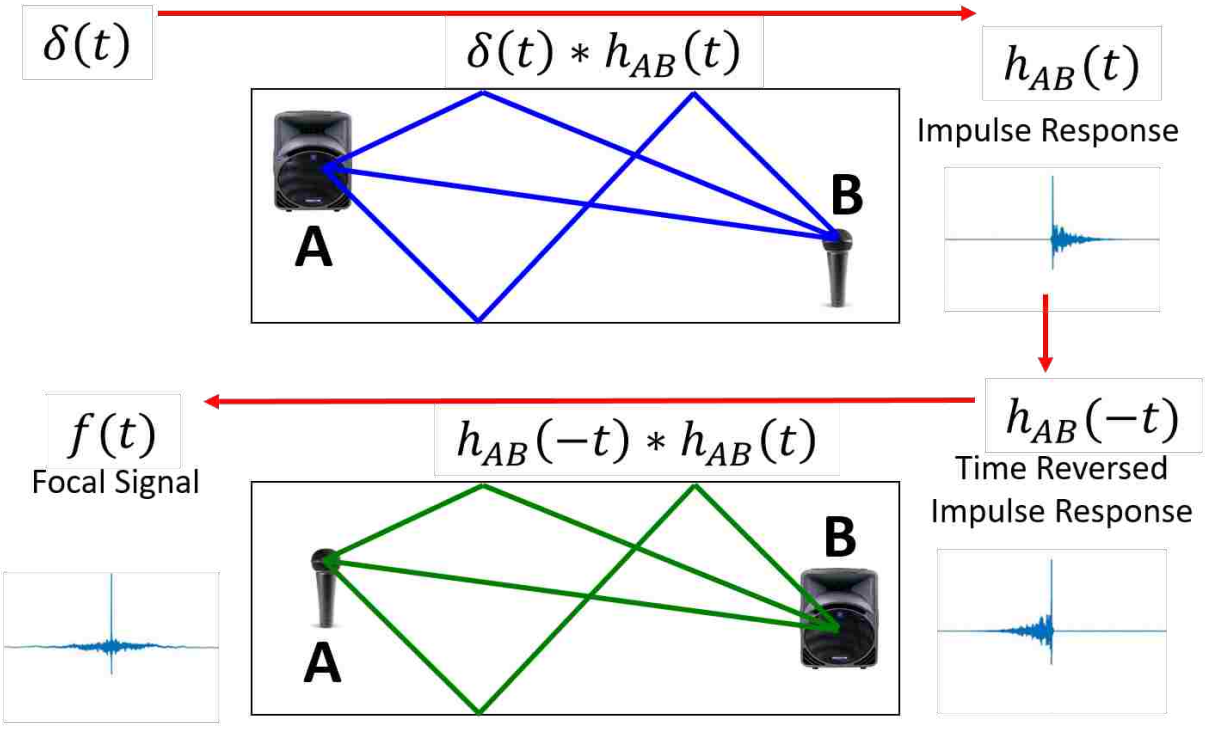

FIG. 1.3. A depiction of standard time reversal with the forward step (top) and the backward step (bottom). $*$ denotes convolution.

Reciprocal TR is much like standard TR except that the locations of the source and receiver are held constant between the forward and backwards steps, as seen in Fig. 1.4. This is possible due to spatial reciprocity. Spatial reciprocity implies that switching the location of the source and receiver does not change the impulse response. The timing of the reflected and direct sound is still maintained, and they coherently combine at the receiver location, B. Reciprocal TR is used throughout this thesis.

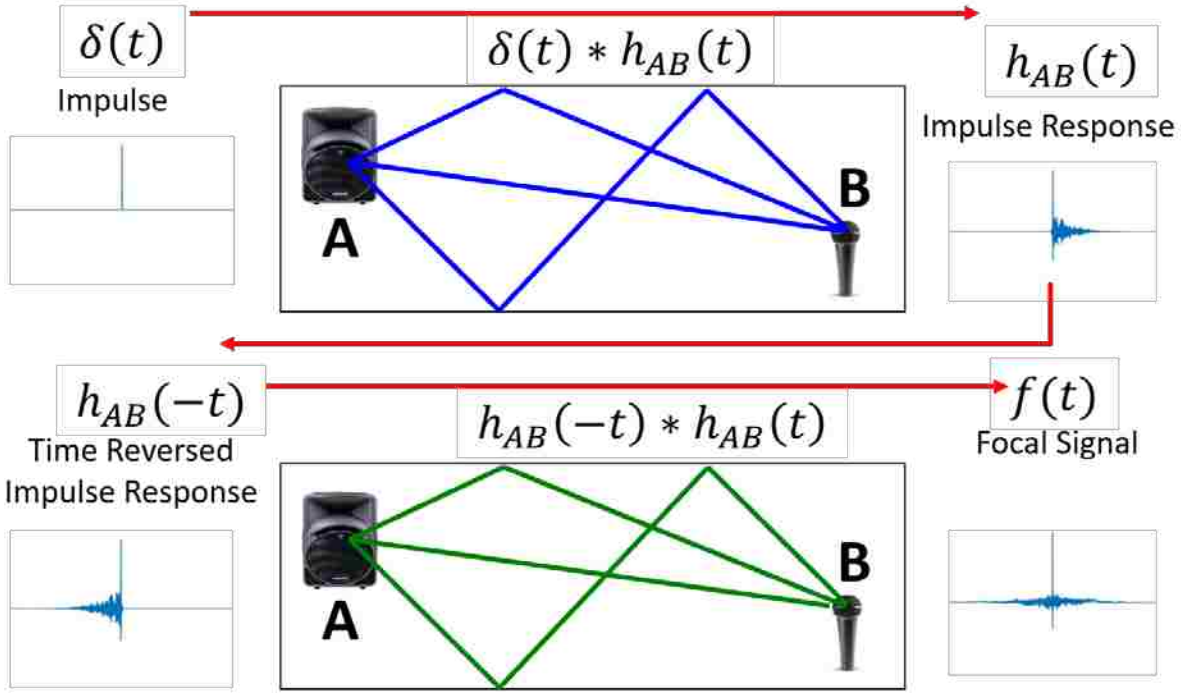

FIG. 1.4. A depiction of reciprocal time reversal with the forward step (top) and the backward step (bottom). $*$ denotes convolution.

As seen in the focal signals in Fig. 1.3 and Fig. 1.4, noise is present before and after the maximum amplitude in the focal signal. Mathematically, this noise is a result of the convolution, $h_{AB}(-t) * h_{AB}(t)$. This convolution is equivalent to the autocorrelation of $h_{AB}(t)$ (see Chapter 2).[15] Physically, this noise is caused by the transducer's inability to record the direction of each incident ray and subsequently control the direction that each ray of sound is emitted. Ideally, when $h_{AB}(-t)$ is broadcast from the source, the part of $h_{AB}(-t)$ containing the direct sound information is only emitted back in the direction in which the direct path between A and B was received. In reality, the direct sound information is allowed to follow every path between A and B, leading to some of this sound energy arriving after the intended focal time. Likewise, the arrival in $h_{AB}(-t)$ containing the information from a ray of sound with multiple reflections follows every path, during

the backward step, including much shorter paths and some energy thus arrives at B before the intended focal time. The combined effect of part of the energy of each ray of sound arriving before and after the intended focal time results in noise that has been termed side lobes.

The use of multiple transducers improves TR focusing.[16] For reciprocal TR and N transducers, the impulse responses ($h_{A_iB}(t)$) must be found between each source transducer location (A_i) and the receiver at the focus location (B). Each impulse response is time reversed and broadcast from the respective source transducer simultaneously. The signals that arrive at B at the expected time of focusing from each appropriately timed reflection and directly from each source transducer, superpose in the field to create the TR focus. At the focus location, B, the TR focusing is created by each signal adding coherently, thus the maximum focal amplitude increases linearly with N. The side lobe amplitudes add incoherently, thus their amplitudes only increase as $\sqrt{N}$, leading to a relative reduction in side lobe level in comparison to the focal amplitude with larger N.

The quality of TR focusing depends on the amount of reflected energy in a room. Rays of sound that reflect off surfaces can be thought of as coming from image sources outside of the room. More images sources can be included by increasing the recording time of $h_{AB}(t)$, and the strength of each image source can be increased by decreasing the absorption at the surfaces. Increasing the amount of and the strength of each image source leads to a greater maximum focal amplitude but also leads to an increased amount of energy in the slide lobes.

The spatial progress of TR focusing in a room using a single source transducer is shown in Fig. 1.5. Each image in the figure depicts the same spatial region with the focus location at its center. The TR source is located far below and to the left of the region shown. Well before the focal time, the region consists of a random sound field. Just before focal time, converging wave

fronts create a nearly-circular, converging ripple surrounding the focus location. The bottom left section of this ripple is higher amplitude than the rest. This is due to the direct sound coming from the source being the strongest contribution to the focusing. The direct sound wave front results in a curved feature whose ends are denoted by ⁎. At the focal time, the converging wave fronts coalesce and result in the maximum focal amplitude. Once again, the direct sound wave front can be seen. Just after the focal time, the previously converging wave fronts begin diverging away from the focus location. Now the direct sound increases the amplitude of the top right section of the nearly-circular, diverging ripple. Well after the focal time, the region once again consists of a random sound field.

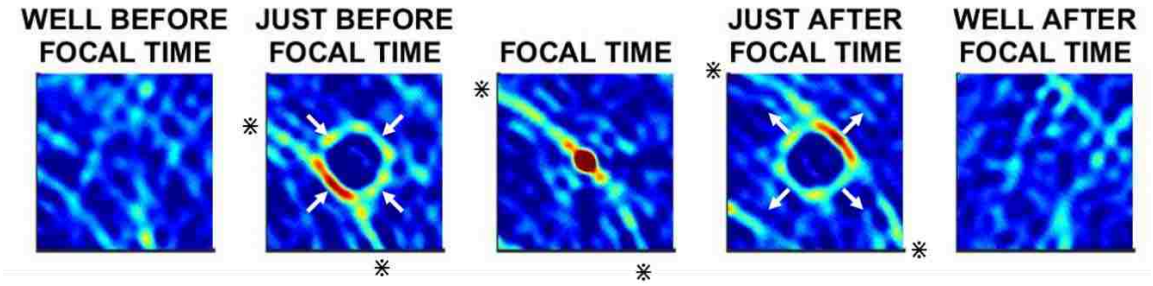

FIG. 1.5. The spatial response showing the progress of TR focusing. The color scale represents the relative pressure amplitude. Arrows denote the direction of wave propagation. ⁎ shows the edges of the direct sound wave front.

TR commonly employs a so-called time reversal mirror (TRM). A TRM is a closely spaced array of transducers often designed to both capture and broadcast wave energy in a standard TR type of experiment. Fink designed an experiment using a TRM that showed how TR benefits from reflected or scattered energy.[3] The experiment consisted of a single underwater source transducer at location *A* and an underwater TRM at location *B*. The source transducer broadcasted an impulse,

and the TRM array recorded the response. The recording was only long enough for each TRM element to record the first arrival of sound; reverberant sound from the water tank boundaries was not included. Individual $h_{AB}(-t)$ signals were then broadcast from each respective TRM element. The resulting signal at the original source location was simply the result of time alignment of each element in the TRM (beamforming). The transducer at A was moved along a line parallel to the TRM to record the spatial extent of the focus. Fink then placed a forest of thin and closely spaced rods between A and the TRM. This provided scattering and created reverberation between the focus location and the TRM. The resulting focus with the forest of rods in place was 6 times narrower spatially than without the rods. Unlike beamforming, where complexities between the array and the focus location could lead to deteriorated focusing, TR benefits from a more complex and scattering-filled environment. However, the system must be linear and time invariant to perform TR focusing.

1.3 Thesis Objective

This thesis aims to understand and improve TR focusing in rooms by performing computer simulations. The results from this thesis will help future researchers understand optimal room and source/focus locations for different applications of TR. Temporal quality (how well TR focuses sound in time) and spatial clarity (how well TR focuses sound in space) are defined and explored for each computer simulation.

Chapter 2 considers the effects that the acoustic absorption and volume of a room enclosure have on TR focusing. It describes how decreasing absorption and/or decreasing volume lead to higher maximum focal response and improved spatial clarity while also leading to lower temporal quality.

Chapter 3 considers the effects that source and focus locations within a room have on TR focusing. For a single source, maximum focal amplitude is increased either by focusing very close to the source or far away from the source. Temporal quality decreases with source/focus location distance while spatial clarity increases. Dual coplanar source and focus locations lead to improving maximum focal amplitude and spatial clarity while lowering temporal quality. For multiple sources, a few different array configurations are considered. The type of array configuration does not have a significant impact on maximum focal amplitude and temporal quality, while a circular array with sources completely surrounding the focus location leads to significantly improved spatial clarity compared to commonly used TRM line arrays.

Chapter 4 provides a conclusion and suggestions for future work. Appendix A contains MATLAB code used for this work. Appendix B contains a description of the software used for the experiments conducted in this work.

Chapter 2

Time Reversal Acoustics Applied to Rooms of Various Reverberation Times

2.1 Introduction

Originally developed for acoustic signal transmissions in the ocean,[1,2] Time reversal (TR) is a process used for focusing wave energy at a particular point in space.[3,4] TR has been used in a variety of acoustics applications, including: high-energy focusing for ultrasound medical operations (i.e. lithotripsy),[5] the reconstruction of source events (i.e., earthquakes),[6] communications in reverberant environments,[7,8,9] and performing nondestructive evaluations of materials.[10,11]

There are two steps to the TR process, the forward propagation and the backward propagation. First, an impulse response (or transfer function in the frequency domain) is obtained between a source and a receiver. Second, the impulse response, $h(t)$, is reversed in time to create the time reversed impulse response, $h(-t)$, which is then broadcast from the source. The response at the receiver is the convolution of $h(t)$ and $h(-t)$ (which is equivalent to the autocorrelation of $h(t)$[15]) and is known as the focal signal. The maximum amplitude of the focal signal is the result of coherent addition of the direct sound between the source and receiver and the reverberant sound arrivals caused by the enclosure. Optimizing the TR process for sound focusing in rooms has been a recent area of research. Some applications require a high amplitude focus, while others require a very narrow and impulsive-like focus. TR in rooms is a fairly new field with a limited amount of

published studies. A brief literature review containing key studies of TR in rooms is included below.

Candy *et al*. studied the feasibility of using TR for an acoustic point-to-point communication experiment in a highly reverberant room.[7,17,18] They found that TR can be used to recover a transmitted information sequence with zero-symbol error. They improved communication quality through the reverberant medium by applying a linear equalization filter, an array of multiple sources, and other signal processing. They did not address how different room conditions might affect TR.

Yon *et al*. performed an experimental study in a reverberation chamber and found that TR provides better temporal and spatial focusing than classical time-delay beamforming because it utilizes the multiple sound paths between the sound sources and focus location.[16] They also found that increasing the number of sound sources and increasing the bandwidth of the impulse response decreases the spatial side lobe level, which results in improved TR focusing. They concluded that side lobe levels are lower in a reverberant room than a free field, but did not define any relationship between reverberation time and TR focusing performance. In their study, a 20-loudspeaker linear array was used to transmit the TR signal, and a single microphone on a one-dimensional scanning system was used to measure the temporal and spatial focus response. They defined a side lobe level as the difference in level between the focal point and the closest measureable side lobe in space.

Ribay *et al*. used a time-domain, finite-difference numerical simulation that was used in previous TR studies in solids[19,20] and related them to room acoustics. They determined that the maximum focal amplitude is $N\tau/\tau_0$, where N is the number of TR transceivers, τ is the reverberation time of the room, and τ_0 is the width of the peak of the focused signal.[21] Thus, any

change to the reverberation time should lead to a linear change in peak amplitude of the focused signal. This relationship is stated but not explicitly shown, numerically or experimentally, in their paper nor in the papers cited.

Anderson *et al*. explored the effect that source directivity has on TR in a room.[14] They found that pointing the loudspeaker source away from the focus location increased the amount of energy in the reverberant field and led to a stronger focal signal amplitude in a highly reverberant room (reverberation time of 6.89 s). However, pointing the source towards the focus location led to a more impulsive like focus (higher temporal focus quality) and a more locally isolated focus (higher spatial focus clarity). In a less reverberant room, with $RT_{60} = 0.65\ s$, the direction of the source did not greatly affect the peak focal amplitude. Thus, the reverberation time of the room, the directivity of the source and direction the source is facing has a dramatic effect of the TR process.

Willardson *et al*. explored the application of TR to produce high amplitude focusing in a reverberant environment.[22] They investigated how TR focusing changed depending on different signal processing strategies applied to $h(-t)$ prior to the backward step of the TR process. When comparing deconvolution, one-bit, clipping, and decay compensation signal processing strategies, they found that clipping produced the highest amplitude focal signal. The experiments were done in a reverberation chamber and did not explore the effects of these processing techniques in different rooms.

The purpose of this paper is to closely study the effects of wall absorption and room volume on the TR process, which is not fully shown in the literature. Numerical simulations and experimental results are used to show that the relationship between maximum focal amplitude and reverberation time given by Ribay *et al*. is true only when reverberation time is changed by

modifying the absorption of the walls in the room.[21] A new relationship between maximum focal amplitude and reverberation time is shown when the reverberation time changes due to changing volume and the absorption is unchanged. Additionally, a temporal quality metric (how well TR focuses sound in time) and a new spatial clarity metric (a new metric that describes how well TR focuses sound in space) are defined and explored for multiple room enclosures. Testing the effects that absorption and room volume have on TR requires many room configurations. Simulations are used to determine the impacts of absorption and room volume on TR focusing due to the practical challenges of performing TR experimentally in many different rooms. However, experimental data are taken in a few rooms to validate the simulated results. Reciprocal TR is used throughout the simulations and experiments.[4]

The image source method is used for the simulations in this study. The method assumes a rectangular parallelepiped room, uniform absorption on all of the walls, frequency-independent absorption (except in Section 2.3.3), omnidirectional and frequency-independent sources and receivers, specular reflections only, and no scattering from objects in the room. Although the inclusion of scattering surfaces has been shown to improve TR focusing,[3] scattering is excluded from the simulations to improve computational efficiency.

2.2 Numeric Acoustic Simulation and TR Metrics

An adequate numerical acoustic simulation for this study must be able to compute an impulse response, $h_{AB}(t)$, between a source at location A and a receiver at location B within a room enclosure (see Fig. 2.1). In the TR process, assuming a frequency-independent source, $h_{AB}(-t)$ is then convolved with $h_{AB}(t)$ to form the focal signal, $f(t)$:

$$f(t) = h_{AB}(-t) * h_{AB}(t) = \int_{-\infty}^{\infty} h_{AB}(-\tau)h_{AB}(t-\tau)d\tau\,, \tag{2.1}$$

$$= R_{h_{AB}h_{AB}}(-t) = R_{h_{AB}h_{AB}}(t).$$

In Eq. 2.1, the $*$ denotes a convolution, τ is an integration dummy variable, and $R_{hh}(t)$ is the autocorrelation of $h(t)$, defined as[23]

$$R_{hh}(t) = \int_{-\infty}^{\infty} h(\tau)h(t+\tau)d\tau\,. \tag{2.2}$$

Because the autocorrelation function is a real and even function, $R_{h_{AB}h_{AB}}(t) = R_{h_{AB}h_{AB}}(-t)$. Thus, the focal signal is simply the autocorrelation of $h_{AB}(t)$.[7,15]

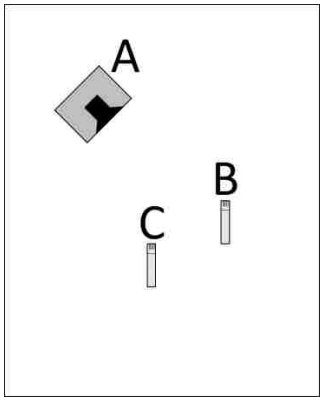

FIG. 2.1. A drawing of a room with a source located at A and microphones located at the focus location B and at the away location C.

To simulate the response at an away location, C, during the backward propagation due to TR focusing at the focus location, B, an away location impulse response, $h_{AC}(t)$, is computed. The response at the away location, $a(t)$, is the convolution between $h_{AB}(-t)$ and $h_{AC}(t)$:

$$a(t) = h_{AB}(-t) * h_{AC}(t) = \int_{-\infty}^{\infty} h_{AB}(-\tau)h_{AC}(t-\tau)d\tau = R_{h_{AB}h_{AC}}(-t). \tag{2.3}$$

Thus the response at an away location, C, is the time-reversed, cross correlation of $h_{AB}(t)$ and $h_{AC}(t)$. Because cross correlations and autocorrelations are much more computationally efficient than convolutions, this paper simulates $f(t)$ by computing the autocorrelation of $h_{AB}(t)$ and $a(t)$ by computing the time-reversed, cross correlation of h_{AB} and h_{AC}.

When experimentally performing TR, it is common practice to normalize $h_{AB}(-t)$ to the maximum input voltage of the amplifier before broadcasting it from the sound source in order to maximize the focal amplitude. Similarly, each simulated $h_{AB}(-t)$ is normalized to have a maximum amplitude of one before convolving it with $h_{AB}(t)$. Thus the autocorrelation and cross correlation results are scaled by the appropriate normalization factor to set the maximum amplitude of $h_{AB}(-t)$ to one.

2.2.1 Image Source Method

The image source method models specular reflections off room surfaces as sound coming from image sources outside of the room. In a closed room, every surface acts as a mirror that creates an image source.[24] For a rectangular parallelepiped room, the parallel surfaces create image rooms that expand out in three dimensions (including diagonal directions) with each having its own image source. Each image source contributes to a specific part of the simulated $h(t)$. During a simulation, all real and image sources simultaneously produce a ray of sound that travels in a straight line between itself and the receiver. The ray loses amplitude according to spherical spreading as it travels. Additionally, every time a ray passes through a wall surface, the ray loses energy according to the wall surface's absorption coefficient. The time at which a ray reaches the receiver is determined by the speed of sound in traveling the distance between the receiver and a

given image source. $h(t)$ is created by linearly superposing the contributions from each ray with the appropriate time delay. Figure 2.2 shows a two-dimensional representation of the image source method with only a few image sources.

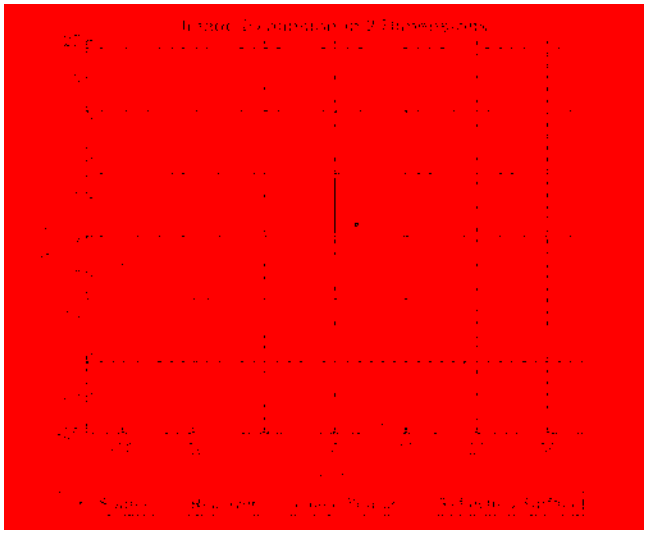

FIG. 2.2. A two-dimensional representation of the image source method. The solid lines represent the original room, while dotted lines represent image rooms. The figure is limited to only a few image sources for simplicity. The actual image space is three-dimensional and includes many more image sources.

The ray tracing method was also considered for this study. This method models sound as following multiple rays that expand in different directions from a source. The rays interact with the room by reflecting off surfaces, with some models including scattering instead of just specular reflections, and some of the sound energy being absorbed according to the absorption characteristics of each surface. Every ray that passes through the defined receiver region is recorded along with the relative amplitude and time of arrival of the sound waves associated with each ray. Finally the signals are added together to form an impulse response. Ray tracing methods can model the inclusion of irregular room geometries and scattering objects (e.g., tables and

chairs). Ray tracing normally requires millions of rays, or more, for accuracy. Depending on the room size, amount of rays used, and the available computational power, a single impulse response may take several hours to calculate. The results presented in this paper required simulations conducted in many different rooms, corresponding to thousands of impulse responses; thus the inefficiencies associated with ray tracing made it an impractical approach. Additionally, the defined receiver region would limit spatial precision and may affect the exact time of arrival of each ray, which timing is of critical importance in the TR process. The image source method only uses the exact number of rays that reach the microphone within a desired time interval and, thus, it is more computationally efficient.

The Allen and Berkley Image Source Method is an efficient and simple algorithm that can be easily implemented in many computational programs.[25] It is a relatively simple approach to modeling room acoustics and thus possesses certain limitations. The model assumes a rectangular parallelepiped room and, therefore, cannot be used for rooms with complicated geometries. The model also assumes that the room is empty, meaning that it does not account for scattering and absorption of sound from objects in the room. The model assumes an omnidirectional source and receiver, each possessing an idealized flat frequency response. Finally, each of the six surfaces in the room must have uniform, frequency-independent absorption coefficients, meaning that it cannot account for irregular absorption regions on a given wall (like an open window or absorptive panel), and the model is restricted to specular wall reflections (i.e., scattering coefficients of walls are not included). A high pass filter at 500 Hz is used to eliminate nonphysical effects near zero frequency and to stay above a typical Schroeder frequency value for the rooms. Although this approach limits a TR study to simple rooms, it is advantageous over other modeling methods because of its computational efficiency and because there is no need to export data from

commercial software packages to simulate TR focusing. Figure 2.3 shows an example of a one-second impulse response created with this method, $h_{AB}(t)$, and the corresponding focal signal, $f(t)$, and a response away from the focus location, $a(t)$.

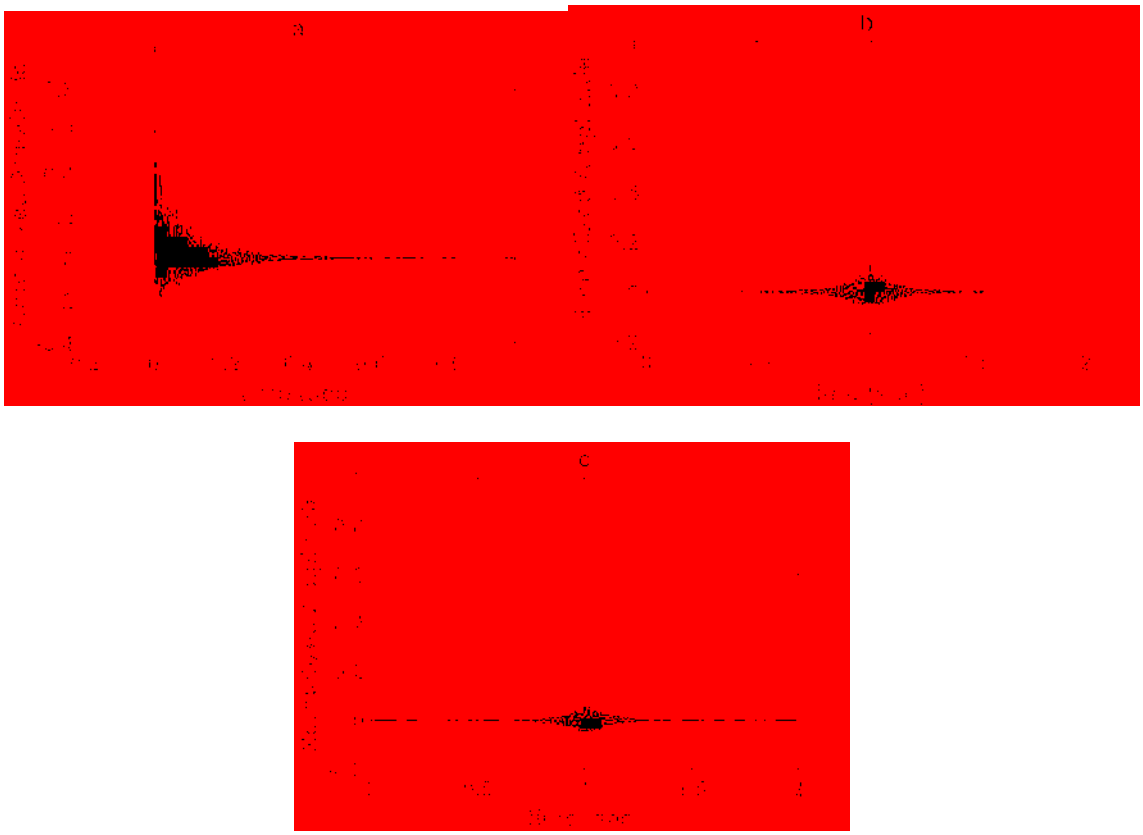

FIG. 2.3. (a) An example of a normalized impulse response generated by the Allen and Berkley Image Source Method. (b) The corresponding normalized focal signal, $f(t)$. (c) A response away from the focus location normalized by the same value as the focal signal, $a(t)$.

The peak energy of the focal signal is located at the center of the focal signal, as seen in Fig. 2.3(b). The side lobes or "noise" appearing before and after the peak energy of the focal signal are a consequence of the autocorrelation and are physically caused by transducers being unable to retrace only the original direct and reverberant sound paths.

Additional work has been done to further improve the original Allen and Berkley Image Source Method. Peterson found that applying a low-pass filter to the impulse response improves arrival time accuracy.[26] A similar approach is followed in this paper by band limiting impulse responses between 500 to 7,500 Hz. The upper frequency limit of 7,500 Hz was chosen based on the results from Willardson *et al.* who found that including frequencies above 7,500 Hz did not greatly impact TR focusing.[22] Additionally, incorporating phase shifts at each sound reflection leads to a better approximation of an impulse response.[27] Unfortunately, incorporating these phase shifts lead to much higher computation time, thus this modification was not incorporated in this study.

2.2.2 Temporal Focus Quality

Many applications of TR require that the focal signals have a narrow temporal envelope. In communications applications, the focal signal is the carrier signal for the intended message. The resulting signal at the focus location is the convolution of the focal signal and the intended message. The ideal, but practically impossible focal signal would be a delta function. This would result in a perfect transmission of the message. The side lobes before and after the maximum amplitude of the focal signal (Fig. 2.3(b)) and the band limited nature of transducers result in asynchronous repetitions of the intended message at the focus location.

Temporal focus quality is a metric that describes how well a focal signal approximates a delta function. It compares the maximum focal amplitude, A_P, with the total energy of the focal signal. While different definitions of temporal quality have been used in the past,[19,22,28,29] this paper uses a modified version of the metric defined by Heaton *et al.*:

$$\xi_T = \sqrt{\frac{[A_P]^2}{\frac{1}{M}\sum_{m=1}^{M}[A(x_0, y_0, z_0, m)]^2}}, \tag{2.4}$$

where $A(x_0, y_0, z_0, m)$ is the amplitude of the mth sample of the focal signal, $f(t)$, at position (x_0, y_0, z_0) and M is the number of discrete samples in the signal A. ξ_T is a unitless metric that, in the case of room acoustics, is effectively the ratio of peak pressure amplitude to the average pressure amplitude of the entire signal. ξ_T is also equivalent to what Derode *et al*. called the signal-to-noise ratio, SNR, which is defined as the peak amplitude divided by the standard deviation of the surrounding noise, σ, or $SNR = \frac{A_P}{\sigma}$.[19]

As an example, the maximum temporal quality possible occurs when the signal is a delta function, which results in $\xi_T = \sqrt{M}$. As seen in Fig. 2.3(b), most focal signals approach zero amplitude at the start and end of the time window. Consequently, ξ_T can be arbitrarily increased or decreased by measuring more or less samples in the recording. Therefore ξ_T is best used as a relative measure of temporal quality of various signals of the same length rather than as an absolute measure of temporal quality.

Equation 2.4 is typically used to calculate ξ_T for the focal signal, $f(t)$, but it can be used to calculate ξ_T for the response at an away location, $a(t)$. This is done by replacing $A(x_0, y_0, z_0, m)$ with $A(x, y, z, m)$, the discrete-time version of the away signal, $a(t)$ at position (x, y, z). A_P is set to the peak amplitude of $a(t)$. ξ_T for the focal signal shown in Fig. 2.3(b) is 94.2 while the away signal shown in Fig. 2.3(c) has a value of 17.1. The higher value of ξ_T for the focused signal is due to a much larger A_P.

2.2.3 Spatial Focus Clarity

Many applications of TR also require that strong temporal focusing only occurs at a single location. For example, in communications applications, it is important that the delivered message is only focused at the intended location and not able to be intercepted at other locations. Spatial focusing metrics have been developed by others to describe the ratio of A_P at the focus location to the amplitudes at other spatial locations.[14,28] Heaton *et al*. also provided a metric for the TR spatial focus quality, ξ_S, that relates the maximum amplitude at the focus location to the amplitude of other locations at the time of maximum focusing.[29] Similarly, Yon *et al*. quantifies spatial focusing using side lobe level, which is the difference between A_P and the largest spatial side lobe amplitude at the focal time.[16]

The spatial focus clarity, Λ_S, is a new metric and is the ratio of temporal quality at the focus point to the average temporal quality over all spatial positions in a two-dimensional region of interest (ROI), and is thus a spatial measure of ξ_T. This metric gives greater insight into the impulsive nature of the temporal signal at the focus location compared to the resulting signals elsewhere. For communication applications of TR, Λ_S can be used to determine the likelihood that the communication might be interpretable elsewhere in the ROI. This paper only considers two-dimensional ROIs along the x-y plane. TR spatial focus clarity is defined as

$$\Lambda_S = \sqrt{\frac{[\xi_T(x_0, y_0, z_0)]^2}{\frac{1}{N_x N_y}\sum_{n_x=1}^{N_x}\sum_{n_y=1}^{N_y}\left[\xi_T\left(n_x, n_y, z_0\right)\right]^2}}, \tag{2.5}$$

where (x_0, y_0, z_0) are the Cartesian coordinates for the focus location, N_x and N_y are the number of measurement locations in the x and y directions respectively in the ROI, and $\xi_T\left(n_x, n_y, z_0\right)$ is the temporal quality at the $\left(n_x, n_y, z_0\right)$ location within the ROI. Λ_S can be made to represent three

dimensions by replacing $\xi_T(n_x, n_y, z_0)$ with $\xi_T(n_x, n_y, n_z)$, multiplying by $\frac{1}{N_z}$ in the denominator and including a third summation over n_z up to N_z. Additionally, Λ_S can be evaluated for two-dimensional ROIs along planes other than the x-y plane by substituting N_x, N_y, n_x and n_y with the appropriate plane variables. Similar to ξ_T, the value of Λ_S can change greatly depending on the values of N_x and N_y and is thus a relative measure of the quality of spatial focusing. Therefore, when comparing multiple TR experiments with different ROIs, each should have the same values for N_x and N_y and grid spacing. Λ_S equals one for anechoic and direct sound exclusive fields because values of ξ_T will be equal at all points in the ROI.

Calculating Λ_S requires the response at every grid location in a ROI due to the source broadcasting $h_{AB}(-t)$. To do this, impulse responses are simulated between the source location and each location, $h_{AC}(t)$, within a ROI and the response is then calculated by computing the time reversed cross correlation between $h_{AB}(t)$ and $h_{AC}(t)$. Figure 2.4 shows the room dimensions along with source, focus, and ROI locations for an example simulation. The room shown is an 8.8 x 11.1 x 7 m rectangular room and the average absorption coefficient of the room is 0.04. The source is located at $(7,6,3)$ m and the focus is at $(4,6,3)$ m with a one-meter ROI around the focus with 2 mm grid spacing for a total of 251,001 ROI grid points, each requiring a unique impulse response. Figure 2.5(a) shows a spatial focus map in dB, which represents the instantaneous sound pressure level (SPL) response at locations within the ROI at the time of maximum focus ranging from -60 to 0 dB (normalized with respect to the SPL value for A_P). The focus location, $(0.5,0.5)$ m, is shown to have the expected maximum response. A feature in Fig. 2.5 that spans along the y direction and near 4 meters in the x direction is shown to have higher than average response. This feature is a result of direct sound coming from the sound source located three meters away, (to the

right as pictured) along the x direction, as seen in Fig 2.4. The high amplitude feature at the focus location is caused by the coherent addition inherent in the TR process.

Figure 2.5(b) shows a map of $\xi_T(n_x, n_y)$ in dB ranging from -30 to 0 dB. The figure shows how ξ_T is maximized at the focus location $(4,6)$ m and how it relates to other locations on the surface, $\xi_T(n_x, n_y)$.

FIG. 2.4. Example room dimensions along with source, focus, and ROI scanning grid locations that were used to simulate the results of Fig. 2.5.

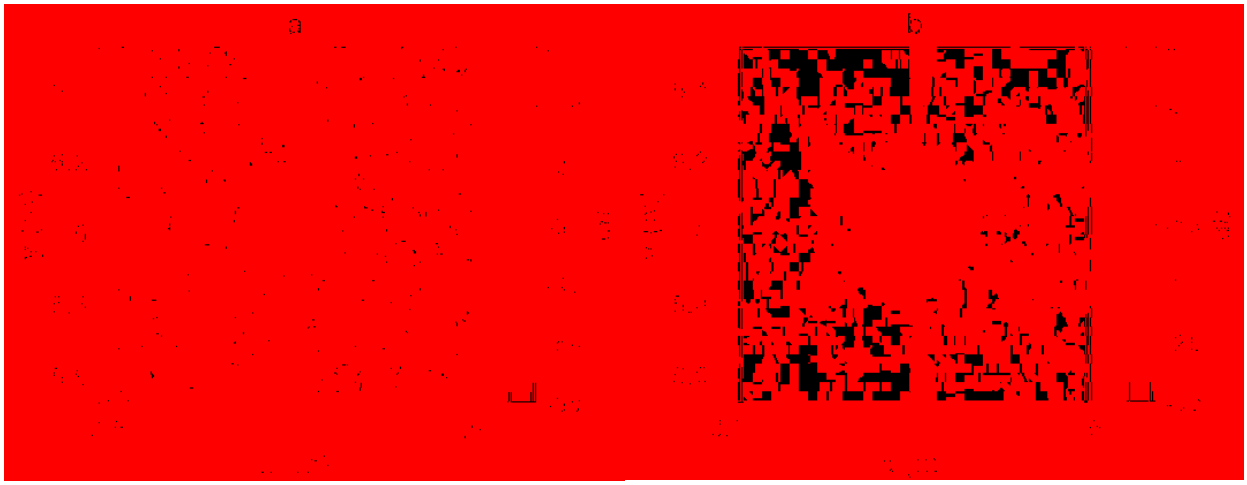

FIG. 2.5. (a) Typical spatial distribution of simulated time reversal focusing in dB re peak. (b) Typical spatial distribution of the temporal focus quality, ξ_T, in dB re peak from simulation results. Note that the sound source is located 3 meters along x to the right from the center of each map.

2.3 Simulated Results

TR simulations were created to more easily determine the effects of wall sound absorption in a room and room volume on A_P, ξ_T, and Λ_S. The Allen and Berkley Image Source Method was implemented in MATLAB in order to simulate impulse responses. Additional filtering was included to limit the frequency range of the impulse responses from 500 to 7,500 Hz which closely resembles the experimental procedures outlined in Section 2.4. Each impulse response was 0.8 s in length and sampled at 50 kHz. Impulse responses recorded longer than 0.8 s did not greatly affect the response across the ROI. The autocorrelation of $h(t)_{AB}$ was used to determine the focal signal. The focal signal was used to calculate A_P and ξ_T according to Eq. (2.4). As seen in Eq. (2.5), Λ_S requires individual values of ξ_T for each location on the ROI. The response at each location was simulated at each grid point in the 1 x 1 m ROI with 10 cm spacing resulting in 121

scanning points. 10 cm spacing was determined to be sufficient to accurately calculate Λ_S for this study, meaning that the trends (shown later on) for Λ_S did not change significantly for finer spacing. Finer spacing would be necessary to study other features of TR focusing, such as the spatial focal spot width. Λ_S is computed for each ROI and then the RT_{60} is changed (either by changing the absorption characteristics of the room or the volume of the room) and the simulation is conducted. Source, focus and measurement grid locations were placed at least 1 m away from any surface to minimize boundary effects and ensure a diffuse field.[30]

2.3.1 Changing Absorption

In order to minimize the likelihood of degenerate modes, a room with an ideal aspect ratio[30] $2^{1/3}:4^{1/3}:1$ with dimensions 3.78 x 4.76 x 3.00 meters and with a uniform absorption coefficient of 0.18 on all six surfaces was used to create the initial simulated room. This room had a predicted RT_{60} of 0.5 s using the Norris-Eyring reverberation formula[31]

$$RT_{60} = \frac{0.161V}{-\ln(1-\langle\alpha\rangle_S)\,S}, \tag{2.6}$$

where V is the volume of the room, $\langle\alpha\rangle_S$ is the absorption coefficient averaged over the room surface area, and S is the surface area of the room, and the factor of 0.161 assumes MKS units and a speed of sound of 343 m/s. To isolate the effect that absorption has on TR, $\langle\alpha\rangle_S$ was systematically lowered (from 0.18 to 0.03) to create 26 simulated rooms such that RT_{60} spans from 0.5 to 3.0 s with 0.1 s increments. The source lactation is (2.34, 2.01, 1.01) m and the focus location is (1.50, 2.85, 1.01) m. For each of the room conditions, A_P, ξ_T, and Λ_S were calculated using the method described previously. Relationships between the Norris-Eyring RT_{60} and A_P, ξ_T, and Λ_S for the 26 rooms are shown by the solid lines of Fig 2.6. For A_P, increasing RT_{60} by decreasing

$\langle\alpha\rangle_S$ leads to a linear relationship between A_P and RT_{60} (coefficient of determination, $R^2 = 0.9997$). This follows the linear relation prediction from Ribay *et al.*[21] Decreasing $\langle\alpha\rangle_S$ also results in a slight lowering of ξ_T and a drastic increase in Λ_S. As RT_{60} changes from 0.5 s to 3 s, A_P increases by 515%, ξ_T decreases by only 2.4% and Λ_S increases by 264%, thus the increases in A_P and Λ_S are much more significant than the decrease in ξ_T. These trends are due to the increased amount of reverberant energy at the focus location as $\langle\alpha\rangle_S$ decreases. For Λ_S, increasing reverberant energy creates a less coherent sound field across the ROI which decreases ξ_T at locations other than the focus. Though not presented here, the same trends were observed when simulating rooms with different volumes.

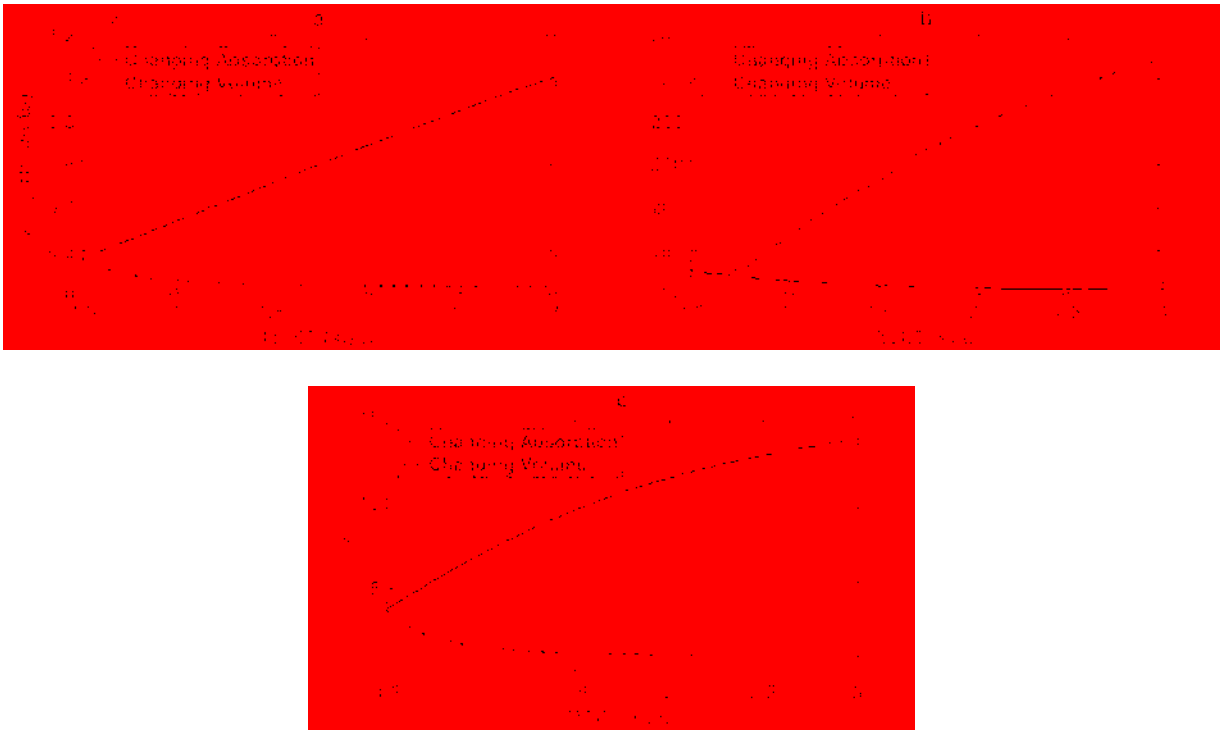

FIG. 2.6. Simulation results for time reversal focusing metrics for various rooms of different frequency-independent absorption coefficients and room volumes. (a) Maximum focal amplitude, A_P, versus RT_{60}. (b) Temporal quality, ξ_T, versus RT_{60}. (c) Spatial clarity, Λ_S, versus RT_{60}.

2.3.2 Changing Volume

The same initial room, as used in Section 2.3.1, with dimensions 3.78 x 4.76 x 3.00 m and with an average absorption coefficient of 0.18 was used to test the effect that changing volume has on TR. Using Eq. (2.6), $\langle\alpha\rangle_S$ was held constant and V was systematically increased to create 26 simulated rooms such that RT_{60} spans from 0.5 to 3 s with 0.1 s spacing. The aspect ratio $2^{1/3}:4^{1/3}:1$ was maintained for every simulated room in order to have a constant relationship between V and S. This resulted in V ranging in values from 54 m^3 for a $RT_{60} = 0.5$ s to 11,664 m^3 for a $RT_{60} = 3$ s. While the simulated rooms increased in size, the source and receiver/focus locations where held at a constant 1.18 m separation but were moved to be located near the geometric center of each room, which effectively resulted in the room expanding out in every direction around the source and focus locations. Figure 2.7 compares a plan view of the room configuration of the initial room with a volume of 54 m^3 and a room with a volume of 2,963 m^3. For each of the room conditions, A_P, ξ_T, and Λ_S where calculated using the method described above. The dashed lines of Fig 2.6 show the relationships between RT_{60} and A_P, ξ_T, and Λ_S.

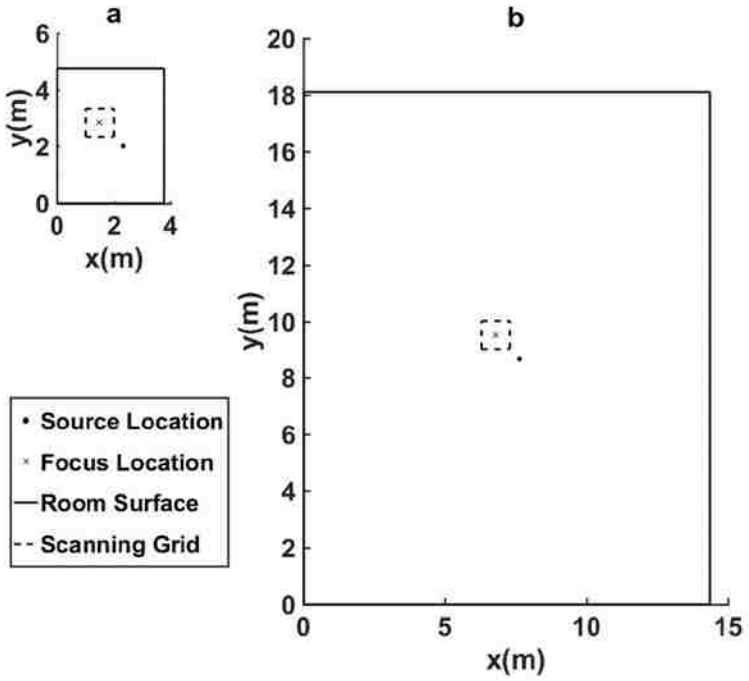

FIG. 2.7. Drawings of two simulated room configurations (a) with a volume of 54 m^3 and (b) with a volume of 2,963 m^3.

Interestingly, increasing RT_{60} by increasing V leads to opposite trends compared to the changing absorption case. Increasing volume leads to lower A_P and Λ_S values and higher ξ_T values. A_P steadily decreases and approaches a minimum value corresponding to the direct sound from the source. Smaller rooms have many early reflections of high amplitude. For larger rooms, the first few reflections arrive later in time and have undergone more spherical spreading loss and thus contribute less to TR focusing. Similarly, Λ_S decreases and approaches a value of one for very large rooms. This is because for larger rooms, an ROI near the source becomes dominated more by the direct sound, which leads to a more uniform response across the ROI. Likewise, ξ_T increases for larger rooms because direct-sound dominated fields lead to more impulsive-like $h(t)$ and focal

signals. As RT_{60} changes from 0.5 s to 3 s due to changing volume, A_P decreases by 80%, ξ_T increases by 26% and Λ_S decreases by 73%.

Contrary to the results of Ribay *et al*., the two distinct trends in Fig. 2.6(a) show that A_P is not always proportional to RT_{60}. For a given room of a fixed volume, changes in absorption follow the trend given by Ribay *et al*. but when the change in RT_{60} is due to volume changes, the trend not only breaks down but there is an apparent opposite trend. This may be because the dependence given by Ribay *et al.* was derived from work in solid media where the losses, aside from spherical spreading, are principally due to propagation absorption losses. In rooms, the losses are principally derived from reflections off wall surfaces and propagation losses are typically negligible in comparison.

2.3.3 Frequency-Dependent Absorption

The original Allen and Berkley Image Source Method creates impulse responses using frequency-independent absorption coefficients.[25] In order to determine if frequency-dependent absorption characteristics of materials affect TR focusing, the image source method was modified to include frequency-dependent absorption coefficients specified at the octave-band center frequencies. This was done by performing the image source modeling with the absorption coefficient corresponding to a given octave band applied to every wall surface. A set of impulse responses for each location within the ROI is obtained. Octave band filtering, using an 8^{th}–order, linear-phase, bandpass filter, is applied to the set of each impulse responses. This process is repeated for each octave-band absorption coefficient, and the impulse responses are filtered for that corresponding octave band of frequencies. After a set of impulse responses is obtained for each octave band, the band pass filtered signals are summed for each location to construct an

impulse response with frequency-dependent absorption properties. It is this constructed set of impulse responses that is then used in the post-modeling simulations of TR. The constructed impulse response is then band limited from 500 to 7,500 Hz to be consistent with the previous sections.

The effects of changing absorption and volume on TR focusing were simulated using frequency-dependent absorption coefficients. Due to the difficulty of finding a wide variety of materials with different absorption characteristics that would lead to incremental changes in RT_{60}, a single material was chosen as a starting point and its frequency-dependent absorption coefficients were multiplicatively changed to produce a desired RT_{60}. Reverse Shroeder integration[32] was used to predict RT_{60} for each constructed impulse response with frequency-dependent absorption coefficients. In this study, gypsum board was chosen for its relatively low-frequency absorption coefficients. These low values permitted a wide range of absorption multipliers allowing for high and low values for frequency-dependent absorption coefficients. Twenty-six multipliers were used, ranging from 0.25 to 8 with logarithmic spacing. Table 2.1 shows seven of the multipliers and the resulting frequency-dependent absorption coefficients ranging from 500 to 8,000 Hz octave bands and the resulting RT_{60} values. After including the frequency-dependent absorption, the constructed impulse response is band limited from 500 to 7,500 Hz to match the previous sections. A multiplier of one results in absorption coefficients equal to gypsum board.[33] The absorption coefficients of materials at 8,000 Hz are not commonly measured, so the value of 0.110 at 8,000 Hz was estimated.

Table 2.1. Octave band frequency dependent absorption coefficients resulting from 7 of the 26 multipliers with the resulting RT_{60}.

	Absorption Coefficients					
Multiplier	**500 Hz**	**1000 Hz**	**2000 Hz**	**4000 Hz**	**8000 Hz**	**RT60 (sec)**
0.250	0.013	0.010	0.018	0.023	0.028	3.61
0.287	0.014	0.011	0.020	0.026	0.032	3.39
		....				
0.871	0.044	0.035	0.061	0.078	0.096	1.83
1.000	0.050	0.040	0.070	0.090	0.110	1.69
1.149	0.057	0.046	0.080	0.103	0.126	1.58
		...				
6.964	0.348	0.279	0.488	0.627	0.766	0.25
8.000	0.400	0.320	0.560	0.720	0.880	0.22

In general, the results from simulations with frequency-dependent absorption shown in Fig. 2.8 are similar to the results with uniform frequency absorption. As before, decreasing absorption leads to higher A_P and Λ_S values and lower ξ_T values. A_P still follows a nearly linear trend with changing absorption (coefficient of determination, $R^2 = 0.9506$), although not as strictly linear as the frequency-independent absorption case. Like before, decreasing $\langle\alpha\rangle_S$ also results in a lowering of ξ_T and a drastic increase in Λ_S. Unique to the frequency-dependent absorption case is a minimum in ξ_T when $RT_{60} = 2$ s. From RT_{60} of 0.2 s to 3.6 s, A_P increases by 3,500%, ξ_T decreases by 16.5% and Λ_S increases by 533%, thus the increases in A_P and Λ_S are again much more significant than the decrease in ξ_T.

For the changing volume case, $\langle\alpha\rangle_S$ is held constant and set equal to the frequency-dependent absorption coefficients of gypsum board. Like before, increasing volume leads to lower A_P and Λ_S values and higher ξ_T values. From a RT_{60} of 1.7 s to 4.7 s, A_P decreases by 92%, ξ_T increases by 35% and Λ_S decreases by 419%.

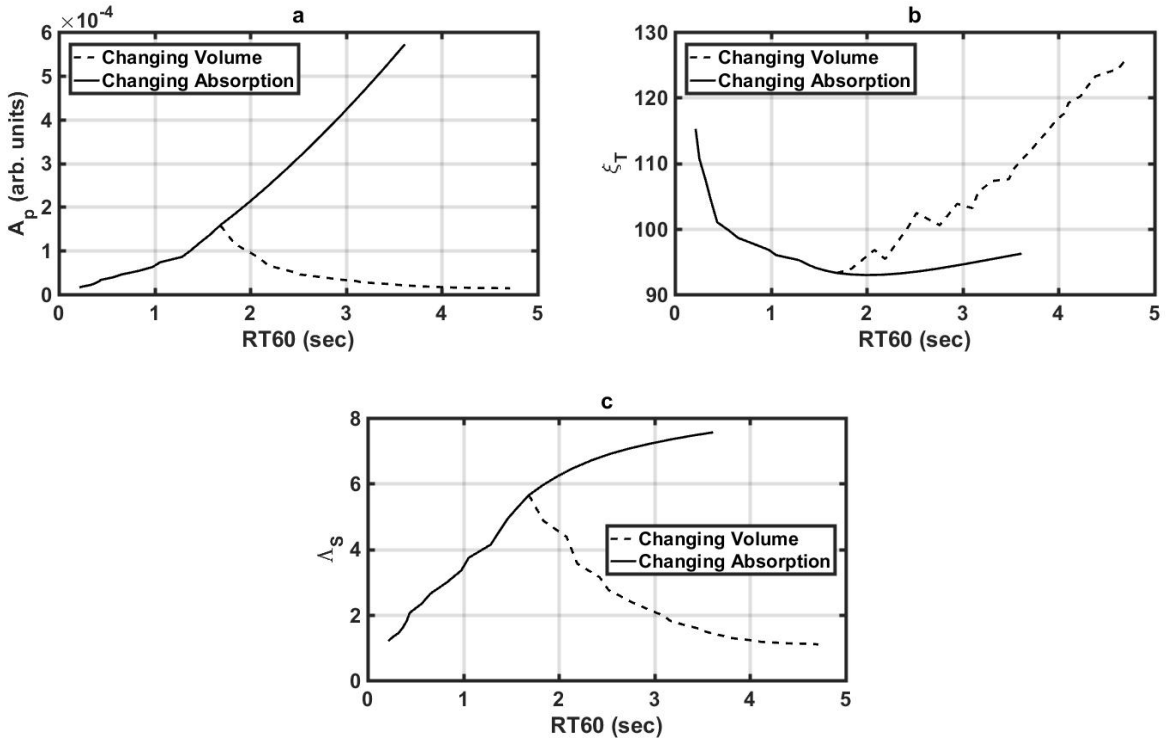

FIG. 2.8. Simulation results for time reversal focusing metrics for various rooms of different frequency-dependent absorption coefficients and room volumes. (a) Maximum focal amplitude, A_P, versus RT_{60}. (b) Temporal quality, ξ_T, versus RT_{60}. (c) Spatial clarity, Λ_S, versus RT_{60}.

In general, the inclusion of frequency dependent absorption in a room does not significantly impact the trends of how changing absorption and volume effect TR focusing. The key trends of increasing A_P and Λ_S and decreasing ξ_T when absorption or volume are decreased still hold.

2.4 Experimental Results

Experimental data was obtained in a few selected rooms in order to compare with the simulated results. This required two types of rooms: one with the ability to incrementally change

the absorption while leaving the volume constant and the other with the ability to change the volume while maintaining constant absorption.

In both experimental setups, a custom built 20 cm diameter dodecahedron loudspeaker, powered by a Crown CT4150 amplifier, was used as the sound source and a G.R.A.S. 46AQ 1.27 cm (0.5 inch) random-incidence microphone, powered by a G.R.A.S. 12AX constant current power module, was used to record the signals. A 14-bit Spectrum M2i.6022 generator was used to generate signals broadcast by the loudspeaker and a 16-bit Spectrum M2i.4931 digitizer was used to acquire the microphone signal with a 50 kHz sampling rate. During the first step of the TR process, a band-limited, three-second duration, linear-chirp signal spanning 500 to 7,500 Hz is broadcast from the dodecahedron loudspeaker, and the microphone records the chirp response. The cross correlation between the chirp signal and the chirp response is used to approximate $h_{AB}(t)$ between the loudspeaker and microphone.[29] $h_{AB}(-t)$ is then calculated, normalized, and broadcast from the loudspeaker. The resulting signal at the microphone is the focal signal. The focal signal is then filtered between 500 and 7,500 Hz with a 8th order, linear phase, bandpass IIR filter to eliminate noise present outside of the excited frequencies. The maximum focal amplitude, A_P, and the temporal quality, ξ_T, are then calculated for each measurement. The spatial extent of the focusing is not measured in these experiments.

2.4.1 Changing Absorption

A reverberation chamber with dimensions 4.96 x 5.89 x 6.98 m (204 m^3) was used to test the effect that changing absorption has on TR. Twenty-four large foam anechoic wedges (0.30 x 0.30 x 0.95 m) were incrementally added to the floor of the reverberation chamber to lower the reverberation time from 8.1 s down to 1.5 s. However, this absorption could not be applied

uniformly throughout the room, nor was the absorption applied uniformly on one surface within the room. The process outlined in the previous paragraph was followed using five averages for both measuring the impulse response and focal signal. The maximum focal amplitude, A_P, and the temporal quality, ξ_T, were determined for six different amounts of wedges (0, 2, 4, 8, 16 and 24). Reverse Schroeder integration[34] was used to determine each RT_{60} (8.1, 5.7, 4.5, 3.0, 1.8, and 1.5 s respectively). Figure 2.9 shows a photograph of the experimental configuration with 24 wedges.

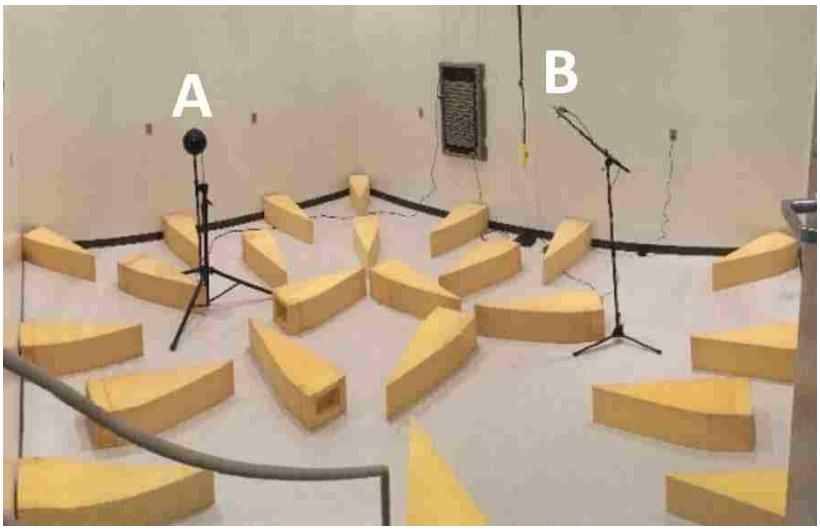

FIG. 2.9. Photograph of the experimental set up in a reverberation chamber with 24 wedges. A is the location of the dodecahedron sound source and B is the location of the random-incidence microphone.

Image source simulations were created for each wedge configuration by increasing the absorption coefficient of only the floor surface (the absorption coefficients for the other 5 walls were held constant) by the appropriate amount to achieve each measured RT_{60}. Figure 2.10 compares simulated with measured A_P with respect to RT_{60}. In the simulations, the amplitudes were uniformly scaled to better match the experimental data trend. These results show the expected

linear trend of A_P with increasing RT_{60} (R^2 = 0.9940), confirming the results shown in Fig. 2.6 pertaining to changing absorption and matching the assertion of Ribay *et al*.[21] The absolute values for ξ_T are greater for the simulated data than the measured data. This is likely due to the sensitivity of ξ_T to noise. According to Eq. (2.4), noise in experimental data increases the summation result in the denominator, leading to a lower value of ξ_T. This also leads to higher values of ξ_T for the noiseless simulations. The simulations of this room suggest there is no dependence of ξ_T on RT_{60}, while the experimental results show a decreasing trend. The reason for this discrepancy is unknown but may be due to the uneven distribution of the foam wedges on the floor in the experimental case, whereas the simulated room had a uniform absorption coefficient for the floor.

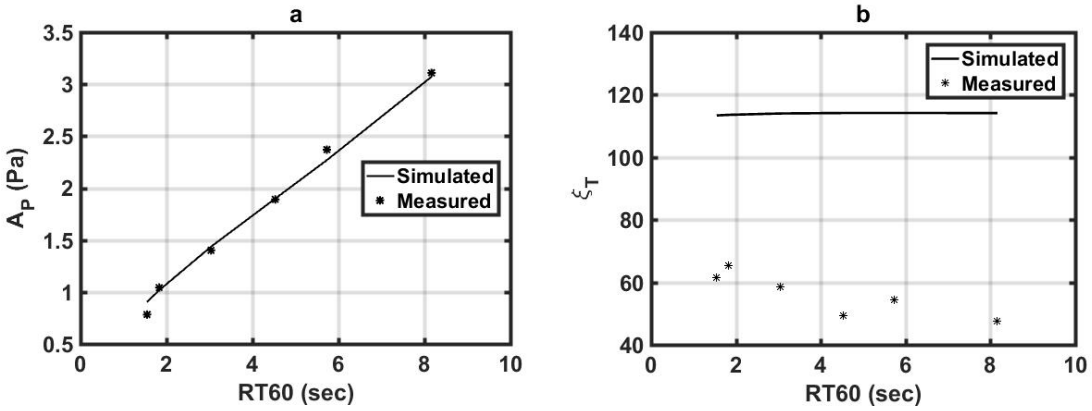

FIG. 2.10. Experimental results obtained in the room shown in Fig. 2.9. (a) Maximum focal amplitude, A_P, versus RT_{60} as a result of changing absorption. (b) Temporal quality, ξ_T, versus RT_{60} as a result of changing absorption with filtered focal signals.

2.4.2 Changing Volume

Experimentally validating the effects that changing volume has on TR required multiple rooms with the same absorption characteristics (or at least similar absorption characteristics) but with different volumes. A multi-purpose room with two room dividers each having high

transmission loss was chosen for its ability to easily change volume while maintaining similar absorption characteristics. With two room dividers, this multi-purpose room allowed for six different volume conditions: three small volume rooms with all room dividers closed, two medium volume rooms with one of the room dividers closed and one large room with all room dividers open. This resulted in the following room volumes: 64, 73, 79, 137, 151 and 215 m^3, which resulted in RT_{60} values of 0.482, 0.485, 0.487, 0.498, 0.499, and 0.502 s, respectively, estimated used Eq. (2.6). Absorption coefficients were estimated using the absorption coefficients of similar building materials found in this room.[34] Figure 2.11 shows an example of one of the medium room configurations with a volume of 137 m^3 with source and receiver locations identified. For each measurement, the dodecahedron loudspeaker and microphone were placed 3.0 m apart. Any changes in the direct sound between source and receiver have an effect on the TR process, thus a constant source to receiver distance is vital to isolating the effects that room volume has on TR. Two measurements were taken in each of the small volume rooms; one with the dodecahedron loudspeaker at the far end of the room and the microphone at the near end of the room (as seen in Fig. 2.11) and the other with the source and receiver positions interchanged. Six measurements were taken in the medium and large volume rooms: two with the midpoint between the loudspeaker and microphone near the center of the room and four with midpoints near the centers of each small volume room that comprises the medium or large volume rooms. Each pair of measurements followed the same loudspeaker and microphone location interchange that occurred in the small volume room measurements.

Figure 2.12 shows the results from the 24 different measurements. Although there is a notable variance in values of A_P for each RT_{60}, there is evidence that mean value of A_P for each room condition decreases with RT_{60} (statistical probability value < 0.0001). This decreasing trend

agrees with the simulation results for the changing volume case displayed in Fig. 2.6 and, thus, also disagrees with the assertion of Ribay *et al*.[21] The experimental and simulation results for ξ_T in Fig. 2.12 agree in that neither has a strong dependence on RT_{60}. From Fig. 2.6, it would be expected that ξ_T should increase with increasing RT_{60}. The apparent discrepancy between the simulation results in Figs. 2.6 and 2.12 may be due to the limited range of values in RT_{60} leading to a limited dataset for ξ_T or the fact that the absorption properties of the room used here did not stay perfectly constant when the volume was increased. The absolute values for ξ_T are greater for the simulated data than the measured data for the same reasons given in Section 2.4.1.

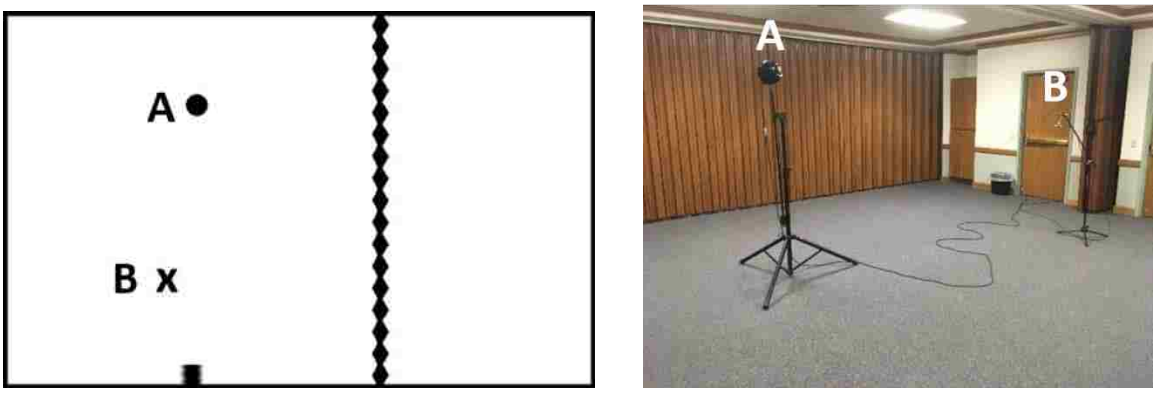

FIG. 2.11. (left) Source A and receiver B locations in a medium room configuration with one room divider closed and the other open. (right) a photograph representing this same configuration where A is the location of the dodecahedron sound source and B is the location of the random-incidence microphone.

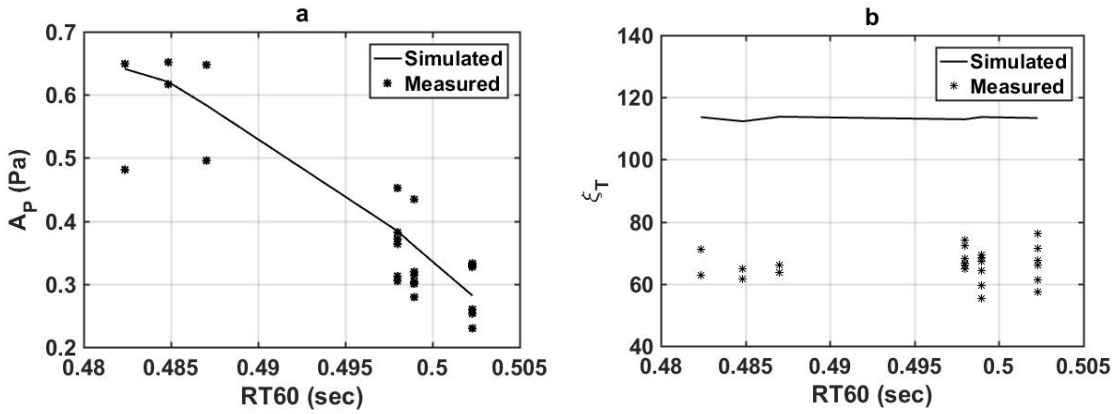

FIG. 2.12. Experimental results obtained in the room shown in Fig. 2.11. (a) Maximum focal amplitude, A_P, versus RT_{60} as a result of changing volume. (b) Temporal quality, ξ_T, versus RT_{60} as a result of changing absorption with filtered focal signals.

2.5 Conclusion

The absorption characteristics and volume of a room have significant and differing impacts on TR focusing. Image source modeling has been used to determine the effects that changing absorption and volume have on maximum focal amplitude, A_p, temporal quality, ξ_T, and spatial clarity, Λ_S. Less absorption increases A_p and Λ_S while decreasing ξ_T slightly. Dissimilarly, larger volumes decrease A_p and Λ_S while increasing ξ_T. The reasons can be traced back to the effect of absorption and volume on the reverberant field and proximity of image sources to the actual source. Higher absorption and larger volumes lead to lower-amplitude reflected arrivals. Higher amplitude reflected arrivals lead to improved A_p and Λ_S and diminished ξ_T, thus smaller, reverberant rooms with high-amplitude early arrivals produce the highest A_p and Λ_S. Limited experimental results confirmed expected trends for A_p. Experimental confirmation of the trends in ξ_T seen in simulated results were limited; further work should be conducted in a more ideal set of rooms.

The relationship between A_p and RT_{60} proposed by Ribay *et al.* was confirmed only if RT_{60} is changed via changing absorption.[21] The relationship is not true if RT_{60} is changed via changing volume. Larger volume rooms with similar absorption characteristics compared to smaller rooms result in lower values of A_p. For larger rooms, the early reflections arrive later in time and have undergone more spherical spreading loss than in smaller rooms and would thus contribute less to TR focusing.

Many TR applications that involve communication of signals require high ξ_T. This paper presents the first known analysis of the effects of room absorption and volume on ξ_T. A decrease in ξ_T indicates a distorted carrier signal for communications, thus it is important to understand what conditions lead to high values of ξ_T. Λ_S is defined for the first time. It is unique in relation to other metrics designed to measure spatial focusing in that it compares the value of ξ_T at the focus location to the values of ξ_T at other locations. This is useful for applications where strong temporal focusing is desired only at the focus location.

Chapter 3

The Effects of Source Placement on Acoustic Time Reversal Focusing in Rooms

3.1 Introduction

For the past 16 years, time reversal (TR) focusing in rooms has been studied within the audible frequency range.[7,14,16,17,18,21,22] Many of these studies have applied concepts learned from underwater applications of TR and from nondestructive evaluation applications of TR to room acoustic applications. These applications often desire at least one of the three main characteristics of TR: a high focal amplitude, narrow temporal focusing and/or tightly confined spatial focusing. The use of multiple TR sources and increased bandwidth have been used to improve all characteristics of TR.[16] Decreasing the absorption in a room or decreasing the volume of a room has led to increased maximum focus amplitude and more precise spatial focusing while decreasing temporal quality somewhat (see Chapter 2).[21]

TR consists of two simple steps, usually referred to as the forward and backward propagation steps. The forward step involves obtaining the impulse response, $h_{AB}(t)$, between the source at location A and the desired focus position at location B. $h_{AB}(t)$ is then time reversed to form $h_{AB}(-t)$. For reciprocal TR, the backward step broadcasts $h_{AB}(-t)$ from the source, which remains at location A.[4] The direct and reverberant sound information contained in $h_{AB}(-t)$ then

retraces their respective paths and coalesces at the focus location (location *B*). The response at the focus location is known as the focal signal.

When multiple TR sources are closely spaced relative to wavelength, the array of transducers is often called the Time Reversal Mirror (TRM).[35,36,37] An advantage to using a TRM is that the direction of arrival of a traveling wave is encoded within the impulse responses of the array if TR elements are spaced within a half of a wavelength. TRMs are commonly composed of linearly spaced elements.[7,16,21] Instead of a closely spaced TRM, Willardson *et al*. placed eight loudspeakers, without consistent, half-wavelength spacing, near boundaries of a reverberation chamber to increase maximum focal amplitude.[22] Likewise, Harker and Anderson found that TR with widely spaced transducers can be used to locate a source in a half-space environment if the source is known to be within a region of certainty.[38]

For single-source acoustic TR, no studies have been found that relate TR characteristics to the distance between the source and focus location in an enclosure. TR characteristics are expected to change significantly with distance between the source and focus location since TR involves the coherent addition of direct sound and reverberant sound. The ratio of the energy of the direct sound to the energy of the reverberant sound changes with the distance between the source and the focus location. Likewise, no studies have been found that recommend optimal source locations and focus locations within a rectangular room. Further, a comparison of different layouts of source transducers used in an enclosure has not been explored in the literature.

The purpose of this paper is to study the effects of source placement on TR focusing in rooms using simulations based on the image source method. For single-source TR focusing, the distance between the source location and the focus location and the arrangement of the source and receiver with respect to the room are considered. Maximum focal amplitude and spatial clarity are

found to increase while temporal quality is found to decrease when the focus location is dual coplanar to the source location in comparison to the source and focus location sharing only one plane. TR focal amplitude is found to be at a minimum when the focus location is at the critical distance and increases closer and farther away from the source while temporal quality steadily decreases and spatial clarity steadily increases farther from the source.

A TRM may not always be feasible nor the ideal layout for every application of TR. For example, sources may be too large to achieve less than half wavelength spacing for the higher frequencies of interest. Different array configurations are considered in Section 3.4.3, including three line arrays with different spacing, a curved arc array, and a circular array that completely surrounds the focus location. The maximum focal amplitude and the temporal quality are not greatly affected by the array type, but a circular array is ideal for maximizing spatial clarity. These findings suggest that the half wavelength spacing of a TRM is not optimal for all applications of TR.

3.2 Numeric Acoustic Simulation

TR simulations of focusing audible sound in rooms can be done using any method that accurately predicts an impulse response. The autocorrelation of an impulse response can be used to represent a focal signal.[7,15] The responses at other locations during TR focusing are needed to determine the spatial clarity. They can be determined by computing the time-reversed, cross correlation of the impulse response, $h_{AB}(t)$, and the impulse response at an away location C, $h_{AC}(t)$. Correlation operations are used because they are more computationally efficient operations than are convolution operations.

This paper utilizes the image source method to calculate impulse responses. The image source method models specular reflections off wall surfaces as sound coming from image sources outside of the room.[24] An impulse response is created by summing together the contributions of many images sources at their respective arrival times. The Allen and Berkley image source algorithm[25] was implemented in MATLAB and impulse responses were band limited between 500 and 20,000 Hz. Full details of the implementations of the image source method are described in Section 2.2.1.

3.2.1 Temporal Quality

Temporal quality is a metric that compares the energy in the peak amplitude of the focal signal, A_P, to the average energy of the focal signal,[22,28]

$$\xi_T = \sqrt{\frac{[A_P]^2}{\frac{1}{M}\sum_{m=1}^{M}[A(x_0, y_0, z_0, m)]^2}}, \tag{3.1}$$

where $A(x_0, y_0, z_0, m)$ is the amplitude of the mth sample of the focal signal at position (x_0, y_0, z_0) (this corresponds to location B) and M is the number of discrete samples in the signal P. Additional discussion on the proper use of ξ_T and its limiting cases can be found in Chapter 2.

3.2.2 Spatial Clarity

Spatial clarity is a metric that compares the value of ξ_T at the focus location to the values of ξ_T across a region of interest (ROI). This paper only considers two-dimensional ROIs along an x-y plane at height z_0. This metric gives greater insight into the impulsive nature of the signal at the focus location compared to the resulting signals elsewhere. Spatial clarity is defined as

$$\Lambda_S = \sqrt{\frac{[\xi_T(x_0, y_0, z_0)]^2}{\frac{1}{N_x N_y}\sum_{n_x=1}^{N_x}\sum_{n_y=1}^{N_y}\left[\xi_T\left(n_x, n_y, z_0\right)\right]^2}}, \tag{3.2}$$

where (x_0, y_0, z_0) are the Cartesian coordinates for the focus location, N_x and N_y are the amount of measurement locations in the x and y directions respectively, and $\xi_T\left(n_x, n_y, z_0\right)$ is the temporal quality at a given location, $\left(n_x, n_y, z_0\right)$. In an anechoic environment, the values of ξ_T across the ROI are constant and Λ_S is equal to one.

3.3 Room Acoustics and Normalization

In room acoustics, the energy density at one location due to a sound source at another is the combination of direct sound field and the reverberant sound field. Hopkins and Stryker developed this expression for the local, average energy density, ρ_{av}, in an enclosure:[39]

$$\rho_{av} = \frac{E}{4\pi c}\left[\frac{\gamma}{r^2} + \frac{16\pi}{R}\right], \tag{3.3}$$

where E is the rate at which the source emits energy, c is the speed of sound, γ is the directivity factor of the sound source ($\gamma = 1$ is assumed for the simulated omnidirectional source and receiver), r is the distance between the source and receiver, and R is the room constant. R is defined as

$$R = \frac{\langle\alpha\rangle_S\, S}{1 - \langle\alpha\rangle_S}, \tag{3.4}$$

where $\langle\alpha\rangle_S$ is the absorption coefficient averaged over the room surface area and S is the surface area of the room. The term γ/r^2 in Eq. (3.3) represents the direct sound field contribution and follows the inverse square law. The term $16\pi/R$ in Eq. (3.3) represents the reverberant sound field contribution and is constant throughout the enclosure. The distance from the source at which the total field has equal contributions of direct sound field and reverberant sound field can be determined by setting the two terms of Eq. (3.3) equal and solving for r. This distance is known as the critical distance, r_c, and is defined as

$$r_c = \sqrt{\frac{\gamma\, R}{16\,\pi}}. \tag{3.5}$$

When $r < r_c$, the total sound field is dominated by the direct sound field and when $r > r_c$ the total sound field is dominated by the reverberant sound field.

The direct sound and reverberant sound energies can be visualized in impulse responses. A simulated impulse response when the receiver is at a distance $r_c/2$, an impulse response when the receiver is at a distance r_c, and an impulse response when the receiver is at a distance $2r_c$ are shown in Fig. 3.1(a)-(c), respectively. Notice how the initial peak of the signal in Fig. 3.1(a), the direct sound, is much greater than the initial peak of the signal in Fig. 3.1(b) which is greater than the initial peak of the signal in Fig. 3.1(c). This is because the direct sound field contribution is much greater as the receiver is brought closer to the source location. The reverberant sound field that exists after the direct sound peak in all signals from Fig. 3.1(a), Fig. 3.1(b) and Fig. 3.1(c) is expected to have similar amounts of energy in all three signals.

When experimentally performing TR, it is common practice to normalize $h_{AB}(-t)$ to the maximum allowable voltage input to an amplifier before broadcasting the amplified signal from the sound source in order to maximize the focal amplitude. Similarly, each simulated $h_{AB}(t)$ is

normalized to have a maximum magnitude of one before cross correlating it with $h_{AC}(t)$ or $h_{AB}(t)$. Figures 3.1(d-f) show the normalized versions of the signals in Figs. 3.1(a-c), respectively. The total energy of the normalized signal in Fig. 3.1(f) is the greatest of the three signals. This is due to the direct sound energy to reverberant sound energy ratio being lowest for the signal in Fig. 3.1(c), which results in a greater total energy after the impulse response is normalized. When the reverberant sound field in $h_{AB}(t)$ is larger, the contribution to the focal amplitude due to the reverberant sound field is greater.

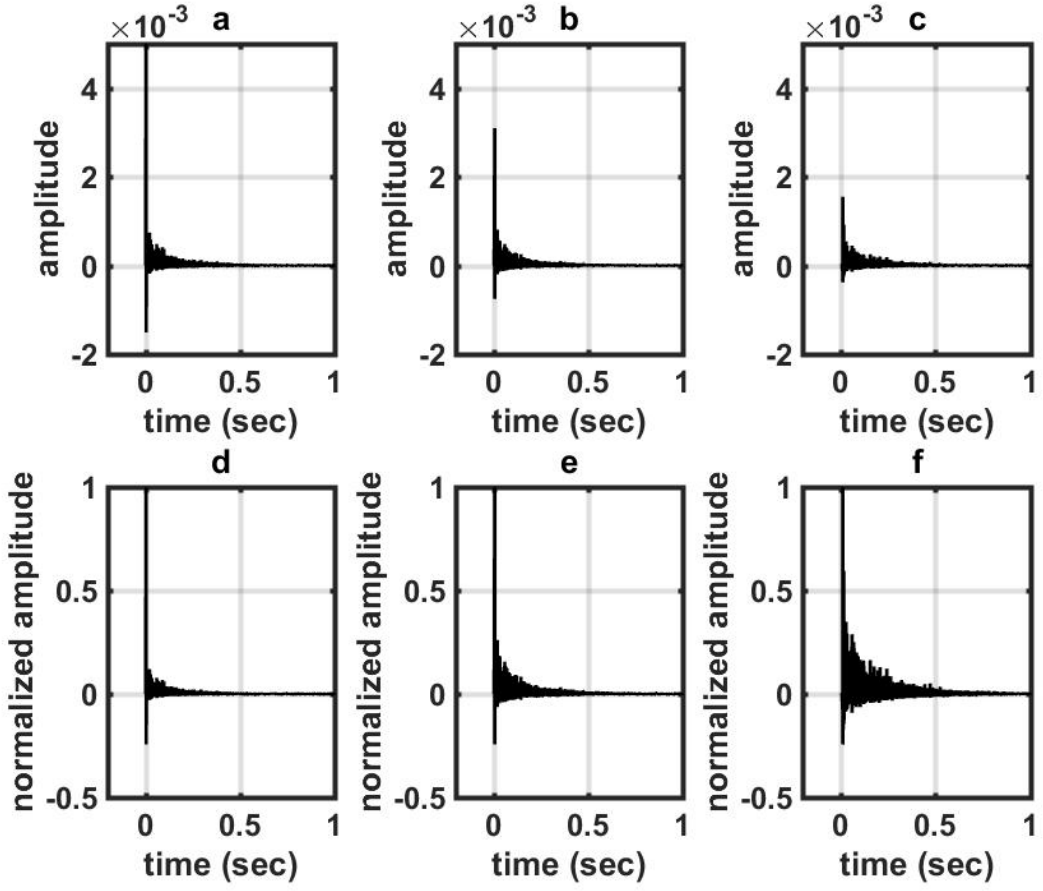

FIG. 3.1. Examples of impulse responses at locations of (a) $r_c/2$, (b) r_c, and (c) $2r_c$ from the source. Plots (d), (e) and (f), respectively, display the normalized impulse responses from (a), (b) and (c).

The amount of energy in the reverberant and direct fields shown in the impulse responses have a direct impact on the resulting focal signal. Figure 3.2 shows different focal signals obtained from using the impulse responses shown in Fig 3.1. Figure 3.2(a) shows a focal signal when the receiver is at a distance $r_c/2$, Fig. 3.2(b) shows a focal signal when the receiver is at a distance r_c and Fig. 3.2(c) shows a focal signal when the receiver is at a distance $2r_c$. Figure 3.2(b) has the lowest A_p.

While viewing the entire focal signals, it is difficult to notice significant differences in the side lobes (energy located on either side of the main focal peak). Differences in the side lobes lead to different values of ξ_T. For this reason, Figs. 3.2(d-f) show normalized and zoomed in views of Fig. 3.2(a-c), respectively. The side lobes of Fig. 3.2(d) are spaced farther apart with less energy between adjacent side lobe peaks. As r_c increases, the distance between side lobe peaks deceases and the energy between prominent side lobe peaks increases. This increased separation leads to a total net increase of energy within the side lobes which should cause a lower value of ξ_T.

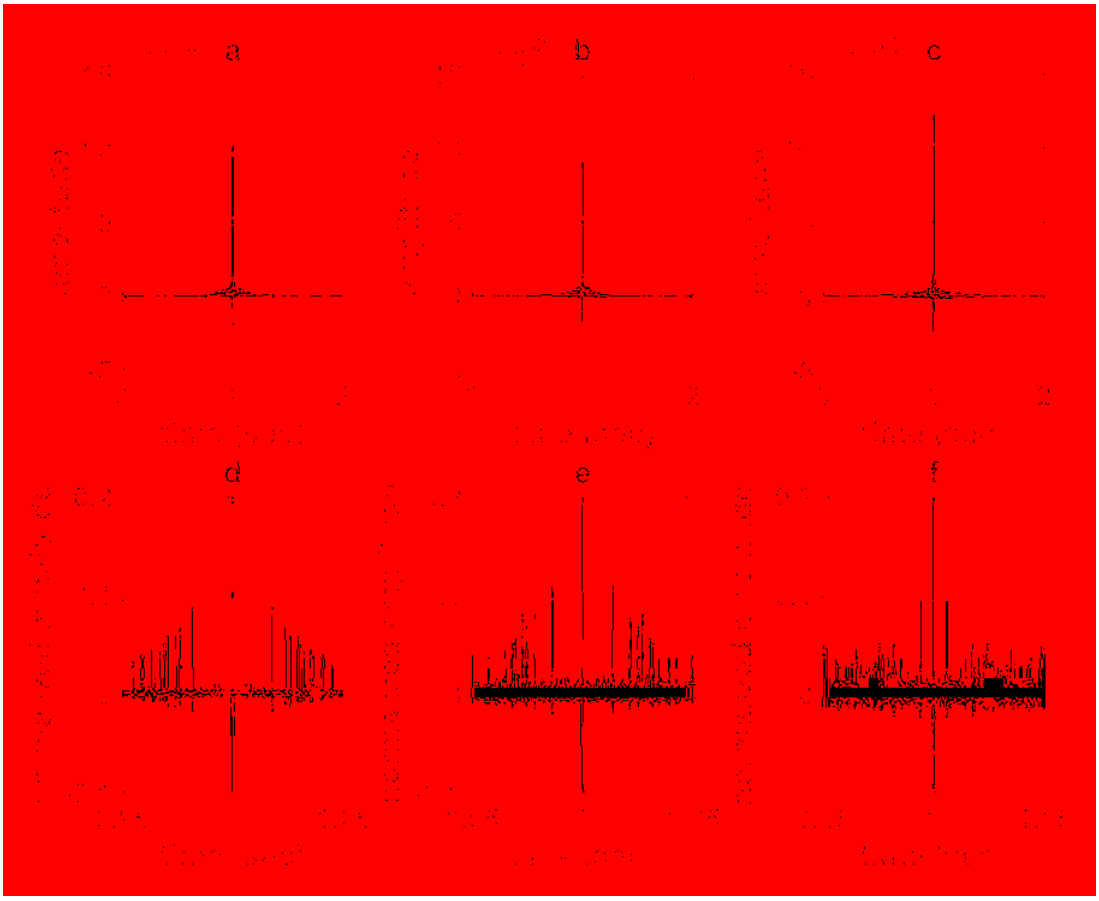

FIG. 3.2. Examples of focal signals at locations of (a) $r_c/2$, (b) r_c, and (c) $2r_c$ from the source. Plots (d), (e) and (f), respectively, display the normalized and narrow views of the focal responses from (a), (b) and (c).

r_c can be easily altered by changing $\langle\alpha\rangle_S$. Changing $\langle\alpha\rangle_S$ will also have a strong effect on the reverberation time, RT_{60}, of a room. This paper predicts RT_{60} using the Norris-Eyring reverberation formula:[32]

$$RT_{60} = \frac{0.161V}{-\ln(1-\langle\alpha\rangle_S)\,S}, \tag{3.6}$$

where V is the volume of the room, and the factor of 0.161 assumes MKS units and $c = 343$ m/s.

Modal effects can cause significant differences in pressure responses for different locations in a reverberant environment. To minimize modal effects, only frequencies in the diffuse field

regime are included. The cut-on frequency for diffuse fields is called the Schroeder frequency, defined as[30]

$$f_S = 2000\sqrt{\frac{RT_{60}}{V}}, \tag{3.7}$$

where the factor of 2000 assumes MKS units. A frequency of 500 Hz is above f_S for all simulated rooms in this paper, and is the reason for the high pass frequency limit specified towards the beginning of Section 3.2. This high-pass limit should ensure that modal effects do not significantly contribute to the spatially dependent focus responses.

3.4 Simulated Results

The Allen and Berkley Image Source Method was used to simulate impulse response for each of the test procedures outlined in this section. In each case, 0.8 s duration impulse responses, sampled at 50 kHz, were simulated. A focal signal was created using the autocorrelation of the impulse response $h_{AB}(t)$. A_P was found and ξ_T was determined using Eq. (3.1). A 1 x 1 m ROI, with 10 cm spacing between points within the ROI, was created with its center at the focus location, resulting in 121 scanning points. 10 cm spacing was determined to be sufficient to accurately calculate Λ_S for this study, meaning that the trends (shown later on) for Λ_S did not change significantly for finer spacing. Finer spacing would be necessary to study other features of TR focusing, such as the spatial focal spot width. The response at each point due to TR focusing was simulated using the time-reversed, cross correlation of $h_{AB}(t)$ and the ROI location impulse response $h_{AC}(t)$. Λ_S was computed for each ROI using Eq. (2).

3.4.1 Distance from Source

A room with 12.6 x 15.9 x 10.0 m dimensions with a uniform average absorption coefficient of 0.35 was created. The resulting $r_c = 3.22$ m and $RT_{60} = 0.77$ s. The source location was placed at (8.75, 4.57, 4.51) m. Forty-three focus locations were chosen, evenly spaced between 0.03 m ($0.0093r_c$) and 6.38 m ($1.97r_c$) from the source with 0.15 m spacing. The focus locations traverse at a 45-degree angle along the *x*-*y* plane. Figure 3.3 shows the source location, focus locations, room surfaces, and r_c for this simulation in plan view.

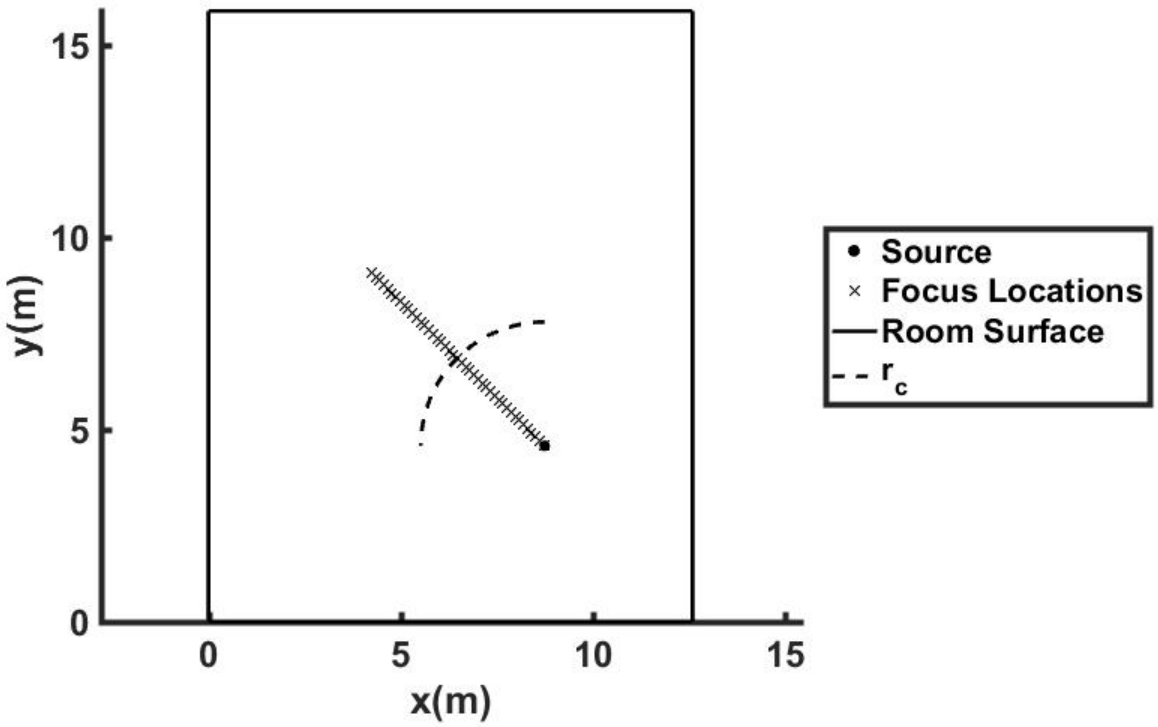

FIG. 3.3. Schematic of the source location, focus locations, room boundaries and critical distance, r_c, used to create the results shown in Fig. 3.4.

TR simulations were performed for each focus location. Figure 3.4 shows the results for A_P, ξ_T, and Λ_S for the focus locations at different distances away from the source. Figures 3.4 (a) shows A_P on a logarithmic scale, and Fig. 3.4 (b) shows A_P on a linear scale and excludes values of r/r_c less than 0.5. The curved trends in Figs. 3.4(a) and 3.4(b) can be attributed to the decreasing influence of the direct sound, the normalization, and r_c. A_P is at a minimum near r_c, where the impulse response and thus the focal signal have equal contributions of direct sound and reverberant sound energy. Since the direct sound field falls off as $\frac{1}{r}$, high A_P is seen for focus locations near the source. As seen in Fig. 3.2, a higher direct sound field to reverberant sound field ratio near the source leads to less energy in the side lobes which causes an increase in ξ_T. However, a strong reverberant field improves the spatial constraint of the focusing, thus focus locations near the source lead to a low value for Λ_S.[3] At distances greater than r_c, the reverberant field dominates and normalization causes the total energy from the source to increase. This increased distance leads to higher values of A_P and increasing values of Λ_S. This is similar to the results found by Anderson *et al*. who found that pointing a directional source away from the focus location can increase A_P;[14] the direct field was decreased by effectively lowering the value of γ in Eq (3.3) and (3.5). In both cases, decreasing the direct sound leads to a relative increase in the reverberant field upon normalization.

A comparison between TR focusing and direct sound emission (i.e., simply outputting an impulse) using the same source, receiver and enclosure as before allows identification of the benefits provided by the addition of TR processing. The same analyses for A_P, ξ_T, and Λ_S are now conducted on the forward propagation impulse responses (instead of analyzing the focal signals) leading to the open-circle results seen in Fig 3.4. The maximum amplitude in the impulse responses are the direct sound, hence A_P is a measure of the direct sound amplitude. Figure 3.4(a) shows that

the values of A_P for locations very close to the source are nearly equal for the TR focusing and direct sound emission. This is due to the strong direct sound contribution to TR focusing when $r < r_c$. For $r > r_c$, A_P for direct sound emission continues to decrease while A_P for TR focusing increases. Direct sound emission at distances below approximately 0.75 r_c have slightly larger values of ξ_T. At larger distances, TR focusing has increasingly larger values of ξ_T compared to direct sound emission. Direct sound emission provides no spatial focusing, thus the values of Λ_S are held constant at one (meaning that the values for ξ_T across the ROI is constant). Increasing the distance results in a greater ratio of reverberant sound energy to direct sound energy, which contributes to improved spatial clarity for TR. Thus, the farther the focus location is away from the source, the more advantageous TR is compared to direct sound emission (with the exception of a slight advantage for direct sound emission in ξ_T for distances below 0.75 r_c).

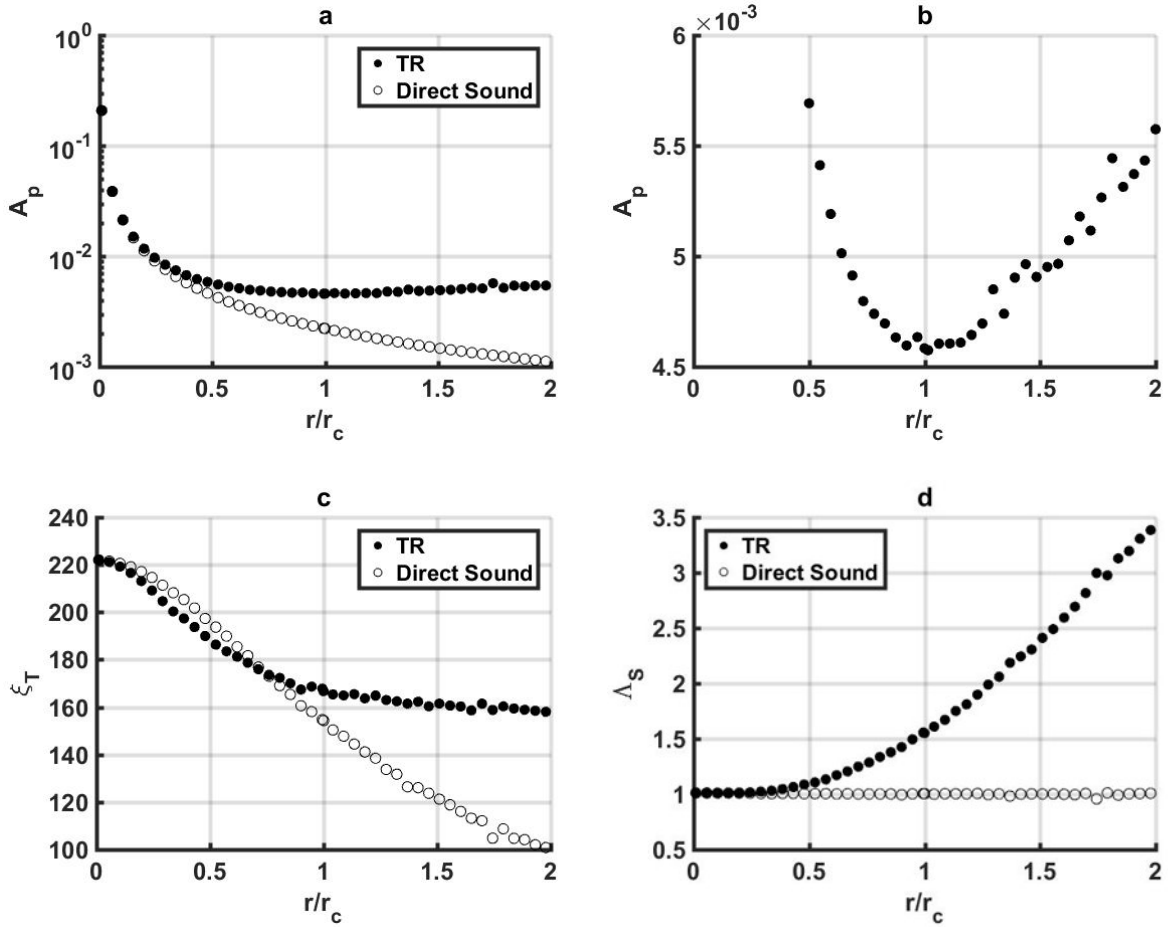

FIG. 3.4. Results of TR focusing (filled circles) and direct sound (open circles) compared to r/r_c for (a) the maximum focal amplitude, A_P, on a logarithmic scale, (b) A_P of TR focusing for values above $r/r_c = 0.5$ on a linear scale, (c) temporal quality, ξ_T, and (d) spatial clarity, Λ_S.

3.4.2 Dual Coplanar Source and Focus

This section explores whether the arrangement of the source and receiver with respect to the room effects TR focusing. A room with 8.8 x 11.1 x 7 m dimensions with a uniform broadband absorption coefficient of 0.18 was simulated, resulting in a room with an $RT_{60} = 1.17$ s and $r_c = 1.44$ m. Ten different arrangements of source/receiver locations were used and averaged together to form the results. As seen in Fig. 3.5, a focus location was chosen and 144 source locations were

placed 2 m ($1.39r_c$) away from the focus location at 2.5° spacing, constituting one of the ten arrangements. For each arrangement, the focus location was located at 3.5 m in the *z* dimension, but its location in the *x* and *y* dimensions were different. The focus location was always 0.5 m away from the center of the room but changed by 36 degrees with respect to the center of the room for each arrangement (see Fig. 3.5(a)) resulting in ten evenly spaced focus locations surrounding the center of the room. For each of the arrangements with its respective focus location, the 144 source locations were placed coplanar with the focus (at the same height) and with the focus at their center (see Fig. 3.5(b)). The average results from these ten arrangements was used in order to eliminate potential boundary effects that could increase or decrease TR focusing.

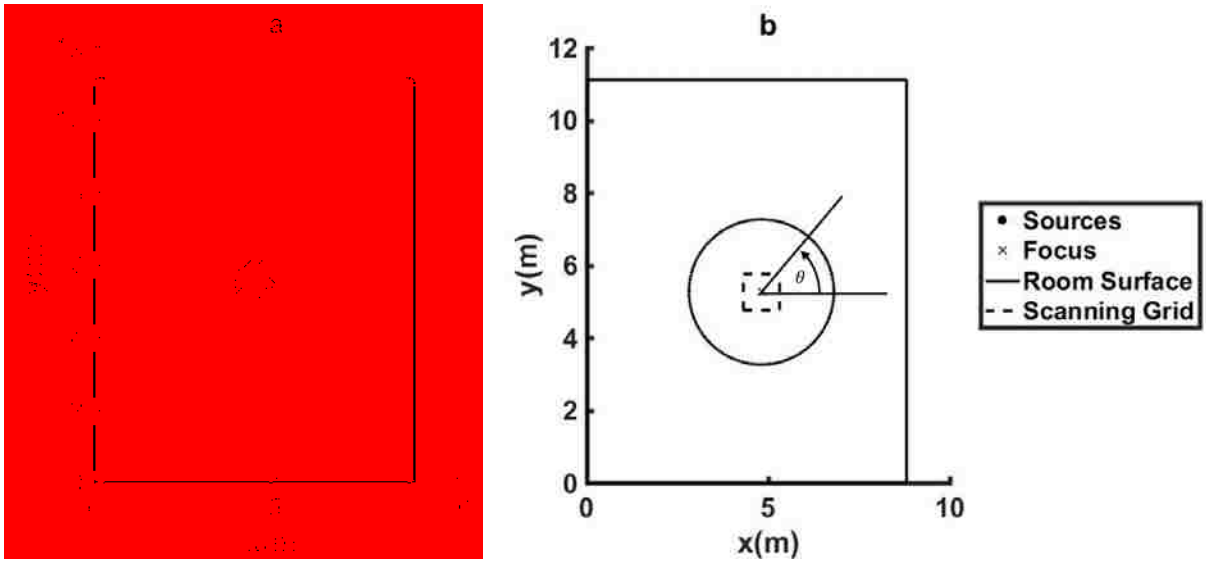

FIG. 3.5. (a) The focus locations for each of the ten source/receiver arrangements. (b) The source locations (closely spaced dots that form a circle), example focus location (x), and ROI scanning grid (dashed box) for a single arrangement. The image in (b) also indicates the zero degree definition (horizontal line) and the direction of increasing angle.

For each of the ten focus location arrangements with their corresponding 144 source locations, A_P, ξ_T, and Λ_S were calculated, with the same size and density ROI as before, centered about each focus location. The average over the ten room arrangements of each of these quantities is shown in Fig. 3.6. For each of these quantities, local extrema exist when a source is located at 0, 90, 180, and 270 degrees (from the perspective of Fig. 3.5(b), directly right, up, left, and down, respectively, towards a wall). The source locations at these angles are coplanar to the focus location in both a *x*-*z* plane (for 0 and 180 degrees) and a *y*-*z* plane (for 90 and 270 degrees) with every source in the simulation being coplanar to the focus location in the *x*-*y* plane. On average, the dual coplanar source locations result in a 20.7% increase in A_P, a 0.6% decrease in ξ_T, and a 7.3% increase in Λ_S relative to these metric values obtained for source locations that were not dual coplanar.

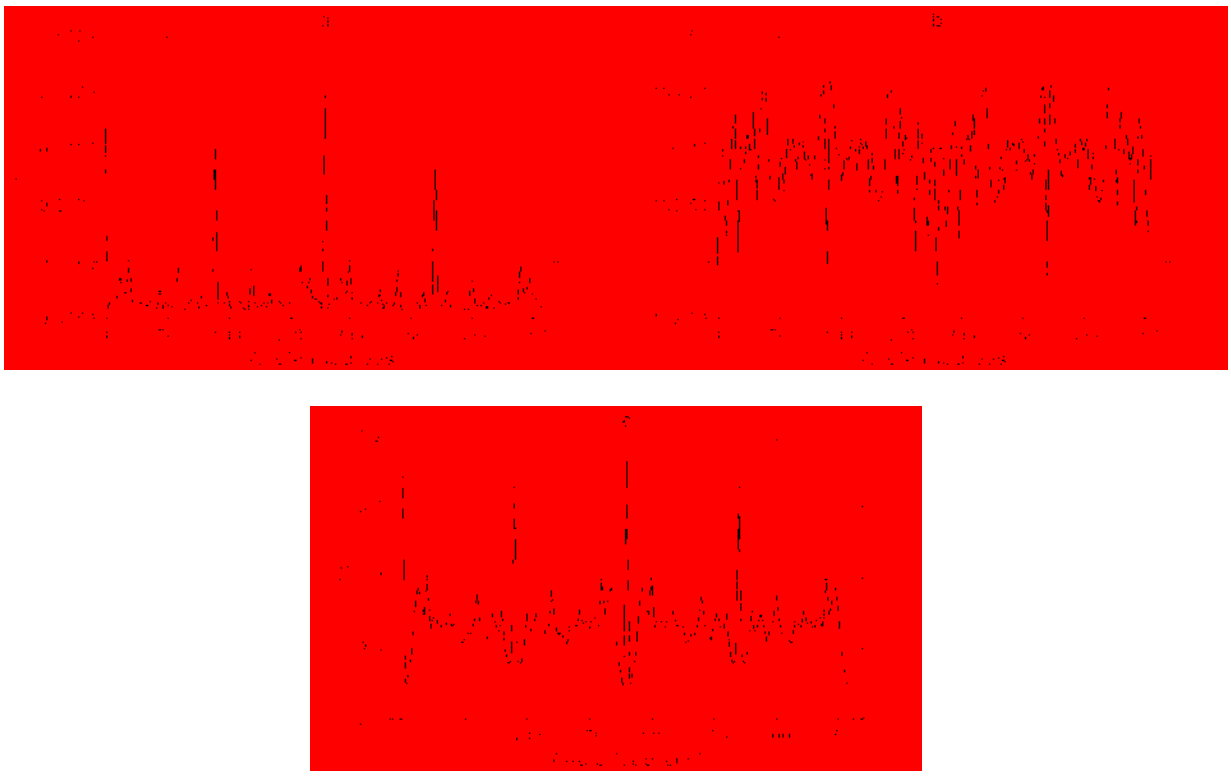

FIG. 3.6. Averaged values over ten source/receiver arrangements as a function of source locations at different angles for (a) maximum focal amplitude, A_P, (b) temporal quality, ξ_T, and (c) Spatial clarity, Λ_S.

The reason for the local extrema of A_P, ξ_T, and Λ_S at dual coplanar source/receiver locations is uncertain. Future work in this area is needed to give further insight into the reasons for these effects. In addition to the findings given in this section, additional simulations not presented in this paper showed that an increase in A_P is observed when the source and receiver are coplanar, in an *x*-*y* plane for example, compared to when the source and receiver do not share a Cartesian plane.

3.4.3 Array Configuration

Five simple array configurations with eight array elements where chosen in order to determine whether the array layout has a significant effect on TR focusing in rooms. For this section, impulse responses were band limited between 500 to 4000 Hz. This bandwidth made the construction of a practical TRM possible, where elements must be spaced less than half the smallest wavelength (4.2 cm in this case).[40] The configurations include a tight line array with 4.2 cm array element spacing forming a TRM, a medium line array with 16.5 cm array element spacing (the same spacing as the array used by Yon *et al*., although their frequency range was 300 to 4000 Hz[16]), a wide line array with 85.7 cm array element spacing, a circular array with array elements evenly spaced circularly around the focus location (45° spacing), and an arc array with 85.7 cm array element spacing following a circular curvature (spanning an arc of 115°). Line arrays are being tested since they are commonly used in TR experiments. The circular and arc arrays are being tested to determine if there are additional benefits to using curved arrays over line arrays. In each array layout, the average distance between each array element and the focus location was 3 m in order to mitigate the source and receiver distance effects outline in Section 3.4.1. Figure 3.7 shows each array configuration relative to the focus and ROI locations.

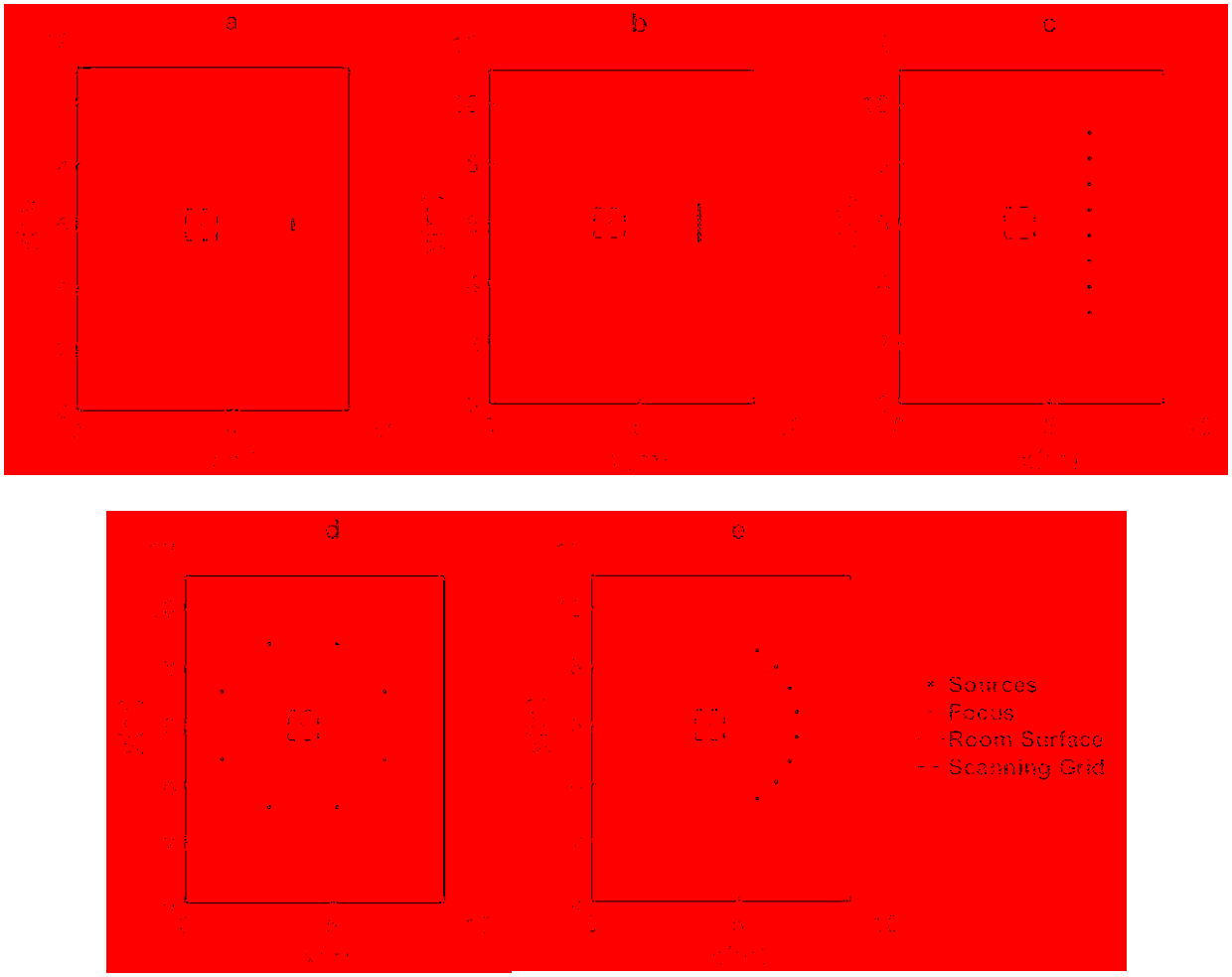

FIG. 3.7. Source, focus and ROI scanning grid locations for (a) tight line array, (b) medium line array, (c) wide line array, (d) circular array and (e) arc array.

A room with 8.8 x 11.1 x 7.0 m dimensions was used with a uniform absorption coefficient. The focus was located at (4, 6, 3) m and the same size and density ROI as before is used, centered around the focus. Each array element was located at a height of 3 m, with x and y location coordinates determined based on the array configuration. Like before, $h_{AB}(t)$ is normalized before computing the autocorrelation for the focal signal or the reversed cross correlation for the away position signal. For each array configuration, four different uniform absorption coefficients were used: $\langle\alpha\rangle_S = 0.79$ which resulted in $RT_{60} = 0.15$ s and $r_c = 6.0$ m , $\langle\alpha\rangle_S = 0.50$ which resulted in

$RT_{60} = 0.35$ s and $r_c = 3.0$ m, $\langle\alpha\rangle_S = 0.11$ which resulted in $RT_{60} = 2.0$ s and $r_c = 1.1$ m, and $\langle\alpha\rangle_S = 0.04$ which resulted in $RT_{60} = 5.7$ s and $r_c = 0.63$ m. The variety of absorption coefficients will help determine whether RT_{60} and the ratio of the distance between the source(s) and the focus location to the critical distance, r/r_c, are factors in the differences in TR results from each array configuration.

Relative standard deviation (RSD) is used to compare variation in TR metric results (A_P, ξ_T, and Λ_S) for each array configuration. RSD is defined as

$$\text{RSD } = \frac{\sigma}{|\mu|} * 100\%, \tag{3.8}$$

where σ is the standard deviation of the data set and μ is the mean value of the data set. A low value of RSD corresponds to a small standard deviation compared to the mean, or that the data is tightly clustered around the mean. A large value of RSD corresponds to a large standard deviation compared to the mean, or that the data is more spread out around the mean. When comparing array configurations, a high value of RSD will correspond to a larger variation between the different array configurations. Low RSD values will signify insignificant differences between the different array configurations.

The TR results A_P, ξ_T, and Λ_S are shown in Tables 3.1, 3.2 and 3.3 show for each array configuration in rooms with the four different values of $\langle\alpha\rangle_S$ and the resulting four values of RSD.

The results for A_P have been normalized to the highest value (circular array in a room with $\langle\alpha\rangle_S$ equal to 0.04). Table 3.1 shows that A_P increases with lower absorption, as expected (see Chapter 2).[21] The largest RSD value for A_P occurs in the room when $\langle\alpha\rangle_S$ is equal to 0.04 and RSD decreases with larger $\langle\alpha\rangle_S$. The array configuration that results in the largest value of A_P is inconsistent between different $\langle\alpha\rangle_S$. For $\langle\alpha\rangle_S$ equal to 0.79 and 0.50, the wide line array created

the largest A_P by a narrow margin, but for $\langle\alpha\rangle_S$ equal to 0.11 and 0.04, the circular array created the largest A_P, also by a narrow margin. The wide line array results in a larger A_P because the middle elements of the array are closer to the focus location than for any other array, a consequence of the choice to have a constant average distance from each element to the focus location for each array configuration. RSD values in Table. 3.1 are all relatively small, thus the array configuration has a small impact on A_P.

Table 3.1. The normalized maximum focus response, A_P, due to each array configuration in four different rooms with different $\langle\alpha\rangle_S$.

	A_P					
$\langle\alpha\rangle_S$	**Tight Line**	**Regular Line**	**Wide Line**	**Circular**	**Arc**	**RSD**
0.79	0.044	0.043	0.044	0.043	0.043	1.06
0.50	0.068	0.068	0.070	0.070	0.070	1.05
0.11	0.382	0.382	0.384	0.398	0.390	1.60
0.04	0.987	0.968	0.958	1.000	0.981	1.61

ξ_T does not significantly change when absorption is changed (see Chapter 2) as shown in Table 3.2. The highest value of RSD for ξ_T occurs when $\langle\alpha\rangle_S$ is 0.50 (which corresponds to $r/r_c = 1$) with a slight decrease when $\langle\alpha\rangle_S$ is 0.79 and a significant decrease at decreasing values of $\langle\alpha\rangle_S$. Unlike A_P, a wide line array consistently results in slightly higher values of ξ_T, again because of

the closer middle elements of this array. Once again, the RSD values are small for each $\langle\alpha\rangle_S$, thus the array configuration has a minimal impact on ξ_T.

Table 3.2. The temporal quality, ξ_T, due to each array configuration in four different rooms with different $\langle\alpha\rangle_S$.

	ξ_T					
$\langle\alpha\rangle_S$	**Tight Line**	**Regular Line**	**Wide Line**	**Circular**	**Arc**	**RSD**
0.79	107.8	110.5	116.4	111.7	111.5	2.03
0.50	100.1	103.9	112.3	106.9	106.9	2.82
0.11	105.9	109.2	110.8	108.4	110.3	0.87
0.04	106.2	110.3	111.0	109.4	110.7	0.54

Λ_S significantly changes when absorption is changed (see Chapter 2) as shown in Table 3.3. RSD values are much higher for Λ_S than for A_P and ξ_T. Like ξ_T, the largest value of RSD for Λ_S occurs when $\langle\alpha\rangle_S$ is 0.50 and decreases with higher and lower values of $\langle\alpha\rangle_S$. The highest value of Λ_S is consistently produced by the circular array with each $\langle\alpha\rangle_S$.

Table 3.3. The spatial clarity, Λ_S, due to each array configuration in four different rooms with different $\langle\alpha\rangle_S$.

	Λ_S					
$\langle\alpha\rangle_S$	**Tight Line**	**Regular Line**	**Wide Line**	**Circular**	**Arc**	**RSD**
0.79	1.07	1.50	1.63	2.22	1.67	15.7
0.50	1.34	1.90	2.34	3.09	2.42	17.5
0.11	3.78	4.37	6.01	6.58	6.00	14.4
0.04	6.20	6.11	7.03	7.12	7.01	6.0

Based on the results from Tables 3.1, 3.2 and 3.3, in general, array configurations make the largest difference in TR focusing for the $\langle\alpha\rangle_S$ =0.5 case. This case corresponds to $r_c = 3$ m, the average distance between the focus location and the array elements. Although some difference in A_P and ξ_T can be attributed to different array configurations, the differences are insignificant. The greatest differences are seen in Λ_S, where, for example, using a circular array can result in up to a 130.6% increase in Λ_S compared to using a tight line array.

These results show that the commonly used, tightly spaced, linear TRM is not necessarily the ideal array configuration for TR focusing in rooms. Arrays with greater angular coverage provide improved Λ_S when compared to tightly spaced arrays. The array configuration has little impact on A_P and ξ_T as long as the mean distances between arrays and the focus location are equal and distances between each array element and the focus location do not greatly deviate from the mean. The reason that arrays with greater angular coverage are optimal for improving Λ_S is because the sources are widely spaced apart and the direct sound from the sources do not beam and form

regions of coherent wave fronts near the focus location, rather they only coherently combine at the focus location.

3.5 Conclusion

This section summarizes the results from Sections 3.4 as a whole and provides detailed strategies for achieving desired TR characteristics (i.e., maximum values for A_P, ξ_T, and/or Λ_S).

3.5.1 Single TR Element

To maximize A_P, the TR focus location should not be placed near r_c from the source. In a reverberant room, this should not be difficult since r_c will likely be very close to the source. The farther the focus location is from r_c, the more reverberant field energy will be created through normalization and the greater A_P will become. Maximizing A_P for a room with low reverberation time requires planning of optimal source placement since r_c is larger in less reverberant rooms. A way to increase A_P would be to focus at a location very close to the source, allowing the strong direct sound field to dominate. However, focusing very close to the source will greatly lower Λ_S, thereby defeating the need for TR processing. In either type of room, focusing to locations that are dual coplanar with the source will also increase A_P.

To maximize ξ_T, the focus location should be very close to the source, again defeating the purpose of using TR processing. This results in an impulse response and focus response that are each dominated by the direct sound. Values of ξ_T may be 28% higher very close to the source compared to far away. Whether the focus location is dual coplanar with the source or not makes little difference in ξ_T.

To maximize Λ_S, the focus location should be as far away from the source as possible, confirming the expected spatial focusing performance that the TR process provides. The decrease in direct sound allows for a more incoherent field throughout the ROI except at the focus location. Λ_S also benefits if the focus location is dual coplanar to the source location.

3.5.2 Multiple TR Elements

The array configuration had little impact on A_P and ξ_T. The highest value of Λ_S was achieved with a circular array, with TR elements completely surrounding the focus location. This array configuration is superior to the commonly used, tightly spaced, linear TRM. For the circular array, the sources are widely spaced apart and the direct sound from the sources do not beam and form regions of coherent wave fronts near the focus location, rather they only coherently combine at the focus location. This results in a high value of ξ_T at the focus location compared to the average value of ξ_T across the ROI, thus resulting in a large value for Λ_S.

Chapter 4

Conclusion

Image source acoustic simulations were used to predict TR focusing in a variety of different rooms with different source and focus location arrangements. Optimal room characteristics, as well as source position and focus location arrangements were found for maximum focal amplitude, A_P, temporal quality, ξ_T, and/or spatial clarity, Λ_S. Decreasing wall surface absorption and/or decreasing room volume leads to higher A_P and improved Λ_S while also leading to lower ξ_T. For a single source, A_P is increased either by focusing very close to the source or far away from the source. ξ_T decreases with source/focus location distance while Λ_S increases. Dual coplanar source and focus locations lead to improving A_P and Λ_S while lowering ξ_T. For multiple sources, the type of array configuration does not have a significant impact on A_P and ξ_T, while a circular array with sources completely surrounding the focus location leads to significantly improved Λ_S compared to commonly used time reversal mirror (TRM) line arrays.

4.1 Impact

A new metric, Λ_S, has been introduced in this thesis. Depending on the TR application, Λ_S may be more useful than existing metrics such as spatial quality or SNR, each of which have been used by others to characterize the spatial focusing of TR at the instant of peak focusing. Λ_S compares ξ_T at the focus location to other locations in a region of interest (ROI). For private speech communication applications, Λ_S may help the researcher understand if the signal is likely to be intelligible at locations other than the focus location.

The results from Chapter 2 confirm the limited findings in the current literature but also go beyond those. Chapter 2 results confirm the relationship between A_P and RT_{60} predicted by Ribay *et al.* when RT_{60} is changed by changing absorption.[21] However, the results of Ribay *et al.* were disproven when one changes RT_{60} by changing volume. In fact the results in Chapter 2 showed a completely opposite trend to the generalization given by Ribay *et al*. Before this study, researchers would have expected a higher A_P in a very large room with similar absorption characteristics to a small room. Here it is shown that A_P will be smaller in the larger room. Researchers now have a better understand how TR focusing in a large room will compare to TR focusing in a small room.

Results from Chapter 3 include the first study of its kind to relate TR focusing to the distance between the source and focus location, r, with respect to the critical distance, r_c, which is a parameter commonly used in room acoustics. This will help researchers determine the optimal r to use in experimental setups to optimize TR focusing. Dual coplanar source and receiver locations are also studied for the first time. Although an explanation for why this would change TR focusing has not yet been found, researchers can nonetheless select appropriate source locations and focus location based on desired TR focusing qualities by whether source locations and focus location are dual coplanar with each other or not.

Finally, Chapter 3 also includes results showing that the commonly used, tightly spaced, linear TRM is not necessarily the ideal array configuration for TR focusing in rooms. Circular arrays that completely encompass the source have greater angular coverage (larger aperture), resulting in improved spatial focusing, without sacrificing A_P or ξ_T. Much of the current literature uses linear TRMs. Researchers can improve their results if they consider using a circular array over a line array.

4.2 Future Work

4.2.1 Experimental results for Chapter 3

Unlike Chapter 2, Chapter 3 is lacking experimental results to compare with the simulated results. Experimental results comparing TR focusing at different distances will require an omnidirectional source and a random incidence microphone, so that $\gamma \approx 1$. A variety of rooms may also be required. For the large BYU reverberation chamber, $r_c \approx 0.29$ m. This short distance makes studying focal signals at $r < r_c$ difficult, however, there will be many locations that can be studied where $r > r_c$. Similar sized rooms to the BYU reverberation chamber with higher absorption such that $RT_{60} = 0.5$ s will result in $r_c \approx 1.37$ m. This type of room will more easily allow for studying focal signals at $r < r_c$. The room constant, R, and, as a result the r_c, are frequency dependent quantities. This may require a band limited $h_{AB}(t)$ that corresponds to r_c over a certain frequency range.

4.2.2 Explore rooms with non-uniform absorption

All simulations in this thesis use equal absorption on the six surfaces of the rectangular parallelepiped with the exception of Section 2.3.3, where different absorption coefficients were chosen to match the experimental setup. A study involving simulated TR focusing in two rooms with the same RT_{60}, one with uniform absorption and the other with one surface that is very absorptive compared to the other five, may lead to different values of A_P, ξ_T, and Λ_S. It is likely that having a single surface that is more absorptive than the rest will lead to a less symmetric converging wave front for TR focusing. This may lead to significant changes in Λ_S.

4.2.3 Source and focus proximity to boundaries

Experimental TR has shown that placing sources near boundaries has increased A_P. This is unsurprising due to expected changes in the radiation impedance of sources near boundaries. Early attempts at simulating this effect proved futile. Sources and focus locations placed near boundaries provided no benefit to A_P according to simulations. These simulations used an alternative filtering method for band-limiting $h_{AB}(t)$. Since radiation impedance changes are not typically modeled with the image source method, it is not anticipated that this effect can be replicated with simulations.

4.2.4 TR focusing in real rooms using simulated $h_{AB}(t)$

One challenge of using reciprocal TR in some applications is the difficulty involved in determining $h_{AB}(t)$. This usually requires a transducer located at location B. In some communications applications, such as private communications in hostile environments, it may be

impossible to have a transducer located at location B, among other potential issues. This will require a new strategy for the forward step of TR. Acoustic simulations could be used to approximate $h_{AB}(t)$ in such environments. If the simulated impulse response, $h_{S,AB}(t)$, accurately predicts the actual $h_{AB}(t)$, it could be used for these applications. Broadcasting $h_{S,AB}(-t)$ would lead to TR focusing at location B. In practice, this may prove to be very difficult. TR focusing is very sensitive to accurate geometry measurements and the speed of sound. Any geometric errors or an inaccurate speed of sound in the simulation may result in a greatly reduced ability to perform TR focusing. This study should include relationships between simulation accuracy and resulting A_P, ξ_T, and Λ_S.

References

[1] A. Parvulescu and C. S. Clay, “Reproducibility of signal transmission in the ocean,” Radio Elec. Eng. **29**, 223-228 (1965).

[2] C. S. Clay and B. E. Anderson, “Matched signals: The beginnings of time reversal,” Proc. Meet. Acoust., **12**, 055001 (2011).

[3] M. Fink, “Time reversed acoustics,” *Phys. Today* **50**(3), 34-40 (1997).

[4] B. E. Anderson, M. Griffa, C. Larmat, T. J. Ulrich, and P. A. Johnson, “Time reversal,” *Acoust. Today* **4**(1), 5-16 (2008).

[5] J-L. Thomas, F. Wu, and M. Fink, "Time reversal focusing applied to lithotripsy," *Utrasounic imaging* **18**(2), 106-121 (1996).

[6] C. S. Larmat, R. A. Guyer, and P. A. Johnson, “Time-reversal methods in geophysics,” *Phys. Today* **63**(8)*,* 31-35 (2010).

[7] J. V. Candy, A. J. Poggio, D. H. Chambers, B. L. Guidry, C. L. Robbins, and C. A. Kent “Multichannel time-reversal processing for acoustic communications in a highly reverberant environment,” *J. Acoust. Soc. Am.* **118**(4), 2339-2354 (2005).

[8] H. C. Song, "An Overview of Underwater Time-Reversal Communication," *IEEE J. Oceanic Eng.* **41**(3), 644-655 (2016).

[9] L. P. Maia, A. Silva and S. M. Jesus, "Environmental Model-Based Time-Reversal Underwater Communications," in *IEEE Access* **6**, 10041-100051 (2018).

[10] B. E. Anderson, M. Griffa, T. J. Ulrich, P.-Y. Le Bas, R. A. Guyer, and P. A. Johnson, “Crack localization and characterization in solid media using time reversal techniques,” *Am. Rock Mech. Assoc.*, #10-154 (2010).

[11] B. E. Anderson, L. Pieczonka, M. C. Remillieux, T. J. Ulrich, and P.-Y. Le Bas, "Stress corrosion crack depth investigation using the time reversed elastic nonlinearity diagnostic," *J. Acoust. Soc. Am.* **141**(1), EL76-EL81 (2017).

[12] C. Dorme, M. Fink, "Focusing in transmit-receive mode through inhomogeneous media: the time reversal matched filter approach," *J. Acoust. Soc. Am.* **98**(2), 1155-1162 (1995).

[13] A. M. Sutin, J. A. TenCate, and P. A. Johnson, "Single-channel time reversal in elastic solids," *J. Acoust. Soc. Am.* **116**(5), 2779-2784 (2004).

[14] B. E. Anderson, M Clemens, and M. L. Willardson, "The effect of transducer directivity on time reversal focusing," *J. Acoust. Soc. Am.* **142**(1), EL95-EL101 (2017).

[15] M. Tanter, J Thomas, and M.Fink, "Time reversal and the inverse filter," *J. Acoust. Soc. Am.* **108**(1), 223-234 (2000).

[16] S. Yon, M. Tanter, and M. Fink, "Sound focusing in rooms: The time-reversal approach," *J. Acoust. Soc. Am.* **113**(3), 1533-1543 (2003).

[17] J.V. Candy, A. W. Meyer, A. J. Poggio, and B. L. Guidry "Time-reversal processing for an acoustic communications experiment in a highly reverberant environment," *J. Acoust. Soc. Am.* **115**(4), 1621-1631 (2004).

[18] A. W. Meyer, J. V. Candy, A. J. Poggio "Time reversal signal processing in communications – A feasibility study," *Lawrence Livermore Nat. Lab. Lib.*, 246245 (2002).

[19] A. Derode, A. Tourin, and M. Fink, "Limits of time reversal focusing through multiple scattering: Long range correlation," *J. Acoust. Soc. Am.* **107**(6), 2987-2998 (2000).

[20] C. Draeger and M. Fink, "One-channel time-reversal in chaotic cavities: Theoretical limits," *J. Acoust. Soc. Am.* **105**(2), 611-617 (1999).

[21] G. Ribay, J. de Rosny, and M. Fink, "Time reversal of noise sources in a reverberation room," *J. Acoust. Soc. Am.,* **117**(5), 2866-28720 (2005).

[22] M. L. Willardson, B. E. Anderson, S. M. Young, M. H. Denison, and B. D. Patchett, "Time reversal focusing of high amplitude sound in a reverberation chamber," *J. Acoust. Soc. Am.* **143**(2), 696-705 (2018).

[23] R. Bracewell, *The Fourier Transform and Its Applications*, 2nd ed. (New York: McGraw-Hill, 1978), pp 46.

[24] J. H. Rindel, "The Use of Computer Modeling in Room Acoustics," *J. Vibroeng.* **3**(4), 41-72 (2000).

[25] J. Allen, and D. A. Berkley, "Image method for efficiently simulating small-room acoustics," *J. Acoust. Soc. Am.* **65**(4), 943-950 (1979).

[26] P. M. Peterson, "Simulating the response of multiple microphones to a single acoustic source in a reverberant room," *J. Acoust. Soc. Am.* **80**(5), 1527-1529 (1986).

[27] E. A. Lehmann and A. M. Johansson, "Prediction of energy decay in room impulse responses simulated with an image-source model," *J. Acoust. Soc. Am.* **124**(1), 269-277 (2008).

[28] T. J. Ulrich, B. E. Anderson, P.-Y. Le Bas, C. Payan, J. Douma, and R. Snieder, "Improving time reversal focusing through deconvolution: 20 questions," *Proc. Meet. Acoust.* **16**, 045015 (2012).

[29] C. Heaton, B. E. Anderson, and S. M. Young, "Time reversal focusing of elastic waves in plates for an educational demonstration," *J. Acoust. Soc. Am.* **141(**2), 1084-1092 (2017).

[30] M. R. Schroeder and K. H. Kuttruff, "On frequency response curves in rooms. Comparison of experimental, theoretical, and Monte Carlo results for the average frequency spacing between maxima," *J. Acoust. Soc. Am.* **34**(1), 76–80 (1962).

[31] ISO 3741:2010, "Acoustics-Determination of sound power and sound energy levels of noise sources using sound pressure—Precision methods for reverberation test rooms" (International Organization for Standardization, Geneva, Switzerland, 2010).

[32] C. F. Eyring, "Reverberation time in 'dead' rooms," *J. Acoust. Soc. Am.* **1**, 217–241 (1930).

[33] ISO 3382:1997(E), Acoustics-Measurement of the Reverberation Time of Rooms with Reference to other Acoustical Parameters (International Organization for Standardization, Geneva, Switzerland, 1997).

[34] D. Davis and C. Davis, *Sound System Engineering*, 2nd ed. (Howard W. Sams & Co., 1987), pp 159.

[35] M. R. Shroeder, "New Method of Measuring Reverberation Time," J. Acoust. Soc. Am. **37**(3), 409-412 (1965).

[36] M. Fink, "Time reversal of ultrasonic fields. Part 1: Basic principles," *IEEE Trans. Ultr. Ferr. Freq. Contr.* **39**(5), 555-566 (1992).

[37] F. Wu, J-L. Thomas, and M. Fink, "Time reversal of ultrasonic fields. Part II: Experimental results," *IEEE Trans. Ultr. Ferr. Freq. Contr.* **39**(5), 567-578 (1992).

[38] D. Cassereau and M. Fink, "Time reversal of ultrasonic fields. Part III: Theory of the closed TR cavity," *IEEE Trans. Ultr. Ferr. Freq. Contr.* **39**(5), 579-592 (1992).

[39] B. Harker and B. E. Anderson, "Optimization of the array mirror for time reversal techniques used in a half-space environment," *J. Acoust. Soc. Am.* **133**(5), EL351-EL357 (2013).

[40] H. F. Hopkins and N. R. Stryker, "A Proposed Loudness-Efficiency Rating for Loudspeakers and Determinatino of System Power Requirements for Enclosures," *Proc. of the IRE.* **36**(3), 315-335 (1948).

[41] M. Fink, "Time-reversed acoustics," Scientific American, Inc. **281**(Nov.), 91-97 (1999).

Appendix A: MATLAB Code for Allen and Berkley Simulations

This appendix includes MATLAB code that can be used to implement the Allen and Berkley image source method for TR simulations. Additional code used to generate all of the figures throughout this thesis can be found on the acoustics shared drive (Z:\Students\Michael Denison\Research\Room Models).

Allen and Berkley Image Source Code

```
function [IR,t] = IRImageMod(RL,R0,R,FS,alpha,NPTS,FP,NN)
% Computes the impulse response of a common source in a rectangular room
% using the Allen and Berkley method

% RL = [lx ly lz] Rooom Dimensions (m)
% R0 = [x0 y0 z0] Source Position (m)
% R = [x y z] Receiver Position (m)
%  alpha  =  [[alphaback  alphaleft  alphadown];[alphafront  alpharight
alphaup]];
% NPTS = number of points of IR to be computed (ex 2^16;)
% FP = Lowpass filter passband frequency. Recommend FP = 20000. If FP =
0,
% then the IR will not be lowpassed.
% NN = filter order (length)
% length of IR is NPTS + N

%                             Front
%                          _____________________
%                         |                     |
%                         |                     |
%              Left       |                     |  Right
%                         |                     |
%                         |                     |
%                       |->_____________________|
%                    (0,0)  ^+Y   +X->
%                             Back


% constants
```

```
      c = 343;
      T = 1/FS;
      IR = zeros(1,NPTS);
      tmax = NPTS/FS;
      dt = T;
      t = 0:dt:tmax-dt;

      % Room Dimensions
      RL = RL/(c*T); %Vector of box dimensions in sample periods

      % Source Position
      R0 = R0/(c*T); %Vector radius to source in sample periods

      % Receiver Position
      R = R/(c*T);%Vector radius to reciever in sample periods

      % Reflection Coefficients (alpha = 1-betta^2) (0 < Beta <= 1)
      betafront = abs(sqrt(alpha(2,1)-1)); betaback = abs(sqrt(alpha(1,1)-1));
%Reflection Coefficients
      betaleft = abs(sqrt(alpha(1,2)-1)); betaright = abs(sqrt(alpha(2,2)-1));
      betaup = abs(sqrt(alpha(2,3)-1)); betadown = abs(sqrt(alpha(1,3)-1));

      Beta = [[betaback betaleft betadown];[betafront betaright betaup]];

      N1 = floor(NPTS/(2*RL(1))+1); %ranges of summation in x
      N2 = floor(NPTS/(2*RL(2))+1); %ranges of summation in y
      N3 = floor(NPTS/(2*RL(3))+1); %ranges of summation in z

      for nx = -N1:N1 % Start summations
          for ny = -N2:N2
              for nz = -N3:N3

                  % LTHIMAGE subroutine
                  DR = R;
                  DR0 = R0;
                  RP = zeros(3,8);
                  I0 = 1;

                  for L =-1:2:1
                      for J = -1:2:1
                          for K = -1:2:1
                              RP(1,I0) = DR(1) + L*DR0(1);
                              RP(2,I0) = DR(2) + J*DR0(2);
                              RP(3,I0) = DR(3) + K*DR0(3);

                              I0 = I0+1;

                          end
                      end
                  end

                  R2L = zeros(1,3);
```

```
                    R2L(1) = 2*RL(1)*nx;
                    R2L(2) = 2*RL(2)*ny;
                    R2L(3) = 2*RL(3)*nz;

                    DELP = zeros(1,8);

                    for I = 1:8
                        DELSQ=0;
                            for J = 1:3
                                R1 = R2L(J)-RP(J,I);
                                DELSQ = DELSQ+R1^2;
                            end
                        DELP(I) = sqrt(DELSQ);

                    end

                    I0=0;

                    for L = 0:1
                        for J = 0:1
                            for K = 0:1
                                I0 = I0+1;
                                ID = round(DELP(I0)+0.5);
                                FDM1 = ID;
                                ID = ID + 1;
                                if (ID > NPTS)
                                else % Contributions from Loss Factors from each
wall
                                    GID            =            Beta(1,1)^abs(nx-
L)*Beta(2,1)^abs(nx)...
                                        *Beta(1,2)^abs(ny-
J)*Beta(2,2)^abs(ny)...
                                        *Beta(1,3)^abs(nz-
K)*Beta(2,3)^abs(nz)/FDM1;

                                    IR(ID) = IR(ID) + GID; % Impulse Response
                                end
                            end
                        end
                    end

                end
            end
        end

        f = FS/100;  % Low pass cutoff at 1 percent of FS
        w = 8*atan(1)*f;
        T = 1/FS;

        R1 = exp(-w*T);
        R2 = R1;
        B1 = 2*R1*cos(w*T);
        B2 = -R1*R1;
        A1 = -(1+R2);
```

```
      A2 = R2;
      Y1 = 0;
      Y2 = 0;
      Y0 = 0;

      for I = 1:NPTS
          X0 = IR(I);
          IR(I) = Y0+A1*Y1+A2*Y2;
          Y2 = Y1;
          Y1 = Y0;
          Y0 = B1*Y1+B2*Y2+X0;
      end

      if FP ~= 0 % Lowpass filter
          N    = NN;         % FIR filter order
          Fp   = FP;        % passband-edge frequency
          Fs   = FS;        % sampling frequency
          Rp   = 0.00057565; % Corresponds to 0.01 dB peak-to-peak ripple
          Rst = 1e-4;        % Corresponds to 80 dB stopband attenuation

          eqnum = firceqrip(N,Fp/(Fs/2),[Rp Rst],'passedge'); % eqnum = vec of
coeffs
      %     fvtool(eqnum,'Fs',Fs,'Color','White') % Visualize filter

          IR = conv(IR,eqnum);
          t = 0:dt:dt*length(IR)-dt;
      end
```

Compute an Impulse Response

```
% An example of generating an impulse response using the Allen and Berkley
% algorithm in the function IRImageMod

clear; close all;

FS = 50000; % Sampling Frequency

lz = 10; lx = lz*2^(1/3); ly = lz*4^(1/3); % Room Dimensions in m
% Ideal Ratio (1:2^1/3:4^1/3)
RL = [lx ly lz]; %Vector of room dimensions (m)

x0 = 3; y0 = 13; z0 = 8; % Source location
R0 = [x0 y0 z0]; %Vector radius to source

x = 8; y = 2; z = 3; % Focus location
R = [x y z]; %Vector radius to focus (m) TEMP

alphafront = 0.15; alphaback = 0.1; % absorption coef. for each surface
```

```
alphaleft = 0.5; alpharight = 0.1;
alphaup = 0.1; alphadown = 0.15;
alpha = [[alphaback alphaleft alphadown];[alphafront alpharight alphaup]];

FP = 20000; % Lowpass frequency
NN = 100; % Lowpass filter order (length)

NPTS = 2^16; % length of the impulse response

[IR,t] = IRImageMod(RL,R0,R,FS,alpha,NPTS,FP,NN); % creates the impulse
% response, IR, and the time array, t.

figure; plot(t,IR)
title('Impulse Response')
xlabel('Time (s)')
ylabel('Amplitude')
grid on
```

Temporal Quality

```
function [Max,TemporalQuality,LargestValue] = FocusQualityT(focus,fs)
% returns max value at focus and temporal quality. Focus is the time
% signal at the focal point.
% Q_t = sqrt([A_p]^2/(T/M*sum([A(x_0,y_0,m)]^2)))

Max = max(focus);
TemporalQuality = sqrt(Max^2/(1/length(focus)*sum(focus.^2)));
LargestValue = sqrt(1/(1/length(focus)));
```

Spatial Clarity

```
function [SpatialQuality,LargestValue] =
FocusQualityS(TemporalQualityArray,x,y,R)

% returns spatial quality value. TemporalQualityArray is an array that
% fits the scanning grid with computed temporal qualities at each point.
% x = array of scan locations in x
% y = array of scan locations in y
% dx and dy are grid spacings in x and y respectively
% R = focus location R = [x,y,z];
% Q_S = sqrt([Q_T0]^2/(Lx*Ly/(Nx*Ny)*sum(sum([Q_T(x,y)]^2)))
% Lx = length in x, Ly in y
% Nx and Ny are number of scan points in x and y respectively
```

```
if length(x)~=1
    dx = x(2)-x(1);
    if length(y) == 1
        dy = dx;
    else
        dy = y(2)-y(1);
    end
else
    dy = y(2)-y(1);
    dx = dy;
end

Nx = length(x);
Ny = length(y);

focusx = find(round(x,4)==round(R(1),4));
focusy = find(round(y,4)==round(R(2),4));

SpatialQuality =
sqrt(TemporalQualityArray(focusx,focusy)^2/(1/Nx/Ny*sum(sum(TemporalQualityAr
ray.^2))));

LargestValue = sqrt(1/(1/Nx/Ny));
```

TR Scan Example

```
% An example of generating an impulse response using the Allen and Berkley
% algorithm in the function IRImageMod and then using it to for TR focusing
% in a room.

clear; close all;

%% define room and IR parameters

FS = 50000; % Sampling Frequency

lz = 10; lx = lz*2^(1/3); ly = lz*4^(1/3); % Room Dimensions in m
% Ideal Ratio (1:2^1/3:4^1/3)
RL = [lx ly lz]; %Vector of room dimensions (m)

x0 = 3; y0 = 13; z0 = 8; % Source location
R0 = [x0 y0 z0]; %Vector radius to source

x = 8; y = 2; z = 3; % Focus location
R = [x y z]; %Vector radius to focus (m) TEMP

alphafront = 0.15; alphaback = 0.1; % absorption coef. for each surface
alphaleft = 0.5; alpharight = 0.1;
```

```
alphaup = 0.1; alphadown = 0.15;
alpha = [[alphaback alphaleft alphadown];[alphafront alpharight alphaup]];

FP = 20000; % Lowpass frequency
NN = 100; % Lowpass filter order (length)

NPTS = 4e4; % length of the impulse response


%% Define ROI grid
px = 1; py = 1; % 1x1m grid
dx = 0.1; dy = 0.1; % grid spacing
x = R(1)-px/2:dx:R(1)+px/2; % x grid
y = R(2)-py/2:dy:R(2)+py/2; % y grid

%% Foward Step
% IRfocus = zeros(length(mult),NPTS+NN);
% IRfocusNorm = zeros(length(mult),NPTS+NN);
% focus = zeros(length(mult),2*(NPTS+NN)-1);

[IRfocus,t] = IRImageMod(RL,R0,R,FS,alpha,NPTS,FP,NN); % computes h_AB(t)
IRfocusNorm = IRfocus/max(IRfocus); % normalizes h_AB(t)

Max = zeros(length(x),length(y));
TemporalQuality = zeros(length(x),length(y));

for m = 1:length(x) % loops over x grid
    for n = 1:length(y) % loops over y grid
        Rscan = [x(m) y(n) z];

        [IRscan,~] = IRImageMod(RL,R0,Rscan,FS,alpha,NPTS,FP,NN); % Impulse
        % response at scanning point, h_AC(t)
        resp = fliplr(xcorr(IRfocusNorm,IRscan)); % The response at
        % location C to the source broadcasting H_AB(-t)
        [Max(m,n),TemporalQuality(m,n),~] = FocusQualityT(resp,FS);
        % Computes the maximum focal amplitude, Max, and temporal quality

    end
end

[SpatialQuality,~] = FocusQualityS(TemporalQuality,x,y,R); % Computes
% Spatial Clarity based off of Temporal Quality values

%% Show Results
mx0 = ceil(length(x)/2);
my0 = ceil(length(y)/2);

Max = Max(mx0,my0);
TemporalQuality = TemporalQuality(mx0,my0);

table(Max,TemporalQuality,SpatialQuality)
```

Appendix B: Tutorial for Performing Time Reversal with the Spectrum Example vi

This appendix demonstrates how to experimentally perform TR using SpectrumExample.vi. This vi program is implemented in LabVIEW and interfaces with 14-bit Spectrum M2i.6022 generator cards and a 16-bit Spectrum M2i.4931 card. It allows for simultaneous broadcast of up to eight channels and recording of up to four channels. Additional details about the block diagram are included to help future researchers modify this vi for their needs.

SpectrumExample.vi Instructions

The vi is only used to broadcast and acquire data. MATLAB is used in conjunction with this vi to perform all of the signal processing. All MATLAB code is included in its own section of this appendix.

The Forward Step

First, chirpgen.m is used to create a linear chirp. Top and bottom frequencies are specified as well as length in time. RT is set to the approximate reverberation time of room. "chirp.wav" is created.

chirp2binsingle.m reads in "chirp.wav" and creates five bin files that can be read into SpectrumExample.vi. They are:

chirpchannel1.bin

chirpchannel2.bin

chirpchannel3.bin

chirpchannel4.bin

zeros.bin

These files contain a chirp going through one channel at a time. Zeros is a file with nothing.

The spectrum example takes the first 1/4 of a signal as channel 1, the second 1/4 as channel 2, etc. Example: chirpchannel1.bin has a sweep followed by silence (needs to be close to the RT of the room) for the first 1/4 of signal. The rest of the signal is blank (so no signal for channels 2-4).

Now, open SpectrumExample.vi. Figure B.1 shows an example of the front panel. To start, load chirpchannel1.bin into card 1 and zeros.bin into card 2 by typing the appropriate text into the File Name (Replay Card 1) and File Name (Replay Card 2) text boxes. The sampling rate for M2i.49xx should be greater than 3000 kHz (this is a result of a bug in the code that I have not been able to resolve, but it is the only way it works). The sampling rate for M2i.60xx should be 50 kHz (or whatever your desired sampling rate is). Mem and Post for M2i.49xx and Mem for M2i.60xx should be set to mem that is outputted from chirpgen.m and chirp2binsingle.m. It represents the amount of samples that will be broadcast and recorded. Reduce gain to an appropriate value for the M2i.60xx card channels. (Begin with less than 500 or so to avoid overloading). Flip the toggle switch (to the right of the plot) for which channel(s) you want to save. Begin the run by clicking on “single” on the top left. Recordings should be saved as "chirpresp(num2str(n))" where n is the n^{th} loudspeaker. Example: "chirpresp1" for the first loudspeaker. Repeat for channels 2-4 by

loading in chirpchannel2.bin into card 1 etc. For channels 5-8 (card 2) load in zeros.bin for card 1 and chirpchannel1.bin for channel 5, chirpchannel2.bin for channel 6 etc. Record each response.

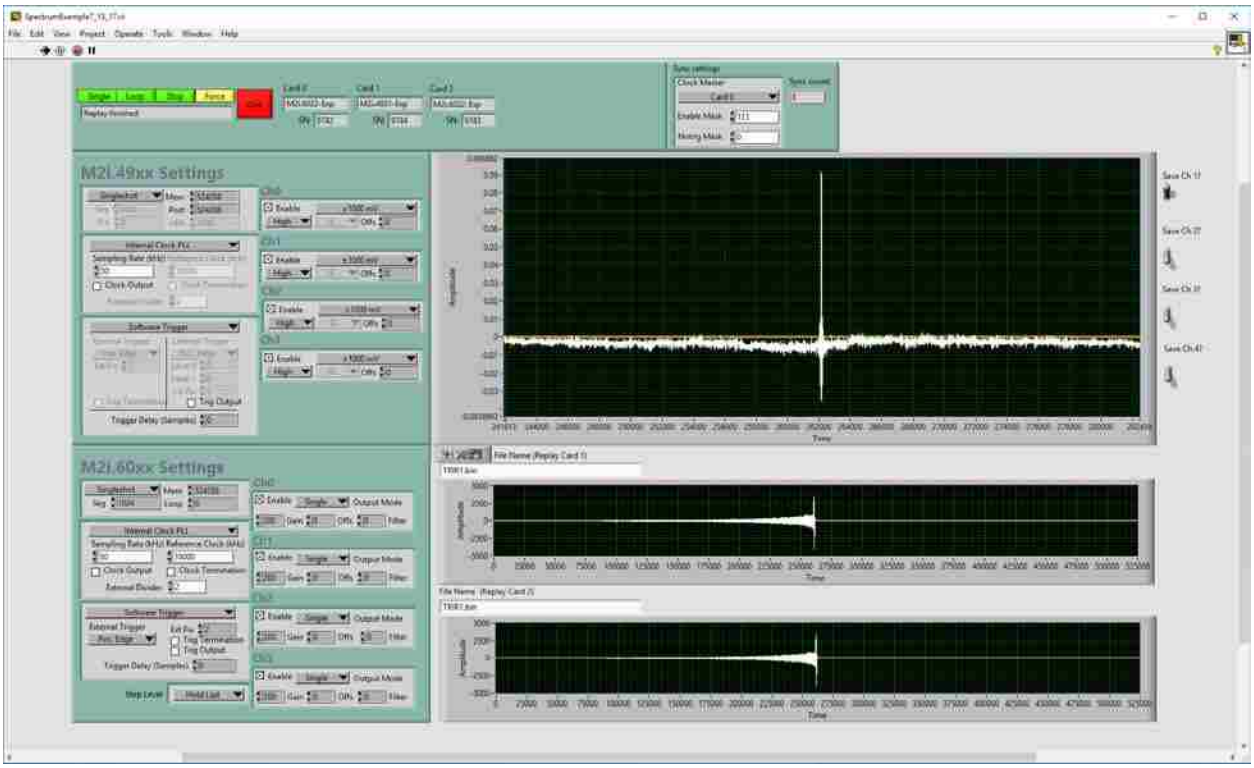

FIG. B.1. The front panel for SpectrumExample.vi. showing the result of TR focusing with eight loudspeakers in a reverberation chamber.

createTRIR_averages.m will be used to load in chirp responses and create "TRIR1.bin" and "TRIR2.bin". Put in the correct IRlength (same as mem from chirpgen.m). Adjust N for the correct amount of loudspeakers used and M for the correct amount of averages (averaging is explained later). Like "chirpcannel(n).bin", "TRIR1.bin" and "TRIR2.bin" have all four signals concatenated together for each card. This file is ready to be loaded into the spectrum example for simultaneously output.

The Backward Step

"TRIR1.bin" and "TRIR2.bin" are then loaded into SpectrumExample.vi. Change Mem and Post for M2i.49xx and Mem for M2i.60xx to the newmem that is outputted from createTRIR_averages.m (should be twice the value of the original mem). Run the vi and save the desired output.

savefocus_averages.m will plot and save the result.

Averaging

Most of the forward and backward steps for incorporating averaging are the same. For M averages, the main idea is to output and record M signals and perform the averaging in MATLAB.

Set M2i.60xx settings from singleshot to continuous. Set Loop to how ever many averages you want (M). Mem and Post in M2i.49xx need to be M*Mem from the M2i.60xx Settings. Save the signal as before (chirpresp1 for example). createTRIR_averages.m reads in the file and performs the averaging. Update M to the amount of averages. Like before, this creates TRIR1.bin and TRIR2.bin for the N channels. After changing Mem to the appropriate value, and Mem and Post in M2i.49xx need to M*Mem, repeat and save the file as "focusresp" like before.

savefocus_averages.m will compute the average and save the result.

MATLAB Code

chirpgen.m

```
% creates a linear chirp.
clear;
```

```
close all;

f1 = 500; % lower frequency 500
f2 = 7500; % upper frequency 7000

fs = 50000; % sampling rate 50000
t = 0:1/fs:3; % length in time of chirp
y = chirp(t, f1, t(end), f2, 'linear',-90); %change phase~~

signaltime = length(y)/fs; %finds length of chirp in seconds
RT = 6; % Approximate reverberation time
totaltime = signaltime + RT; %add RT seconds of reverb
mem = 0;
n=0;
while mem < totaltime*fs
    n = n+1;
    mem = 2^n;
end
mem

zeropad = zeros(1,mem-length(y));

y = [y zeropad];

audiowrite('chirp.wav',y,fs);
```

chirp2binsingle.m

```
% turns chirp.wav into bin files that the spectrum example can use.
clear; close all;
[sample,fs]=audioread('chirp.wav');

mem = 0;
n=0;
while mem < length(sample)
    n = n+1;
    mem = 2^n;
end
mem

post=5000; %maybe wrong name
gain=1;

ch1=int16(post*sample*gain);
ch2=int16(0*sample*gain); % no signal for ch2
ch3=ch2;
ch4=ch2;

data1=[ch1; ch2; ch3; ch4;];
```

```
fileID = fopen('chirpchannel1.bin','w');
fwrite(fileID,data1,'*int16');
fclose(fileID);

ch1=int16(0*sample*gain); % no signal for ch1
ch2=int16(post*sample*gain);
ch3=ch1;
ch4=ch1;

data2=[ch1; ch2; ch3; ch4;];

fileID = fopen('chirpchannel2.bin','w');
fwrite(fileID,data2,'*int16');
fclose(fileID);

ch1=int16(0*sample*gain);
ch2=ch1;
ch3=int16(post*sample*gain);
ch4=ch1;

data3=[ch1; ch2; ch3; ch4;];

fileID = fopen('chirpchannel3.bin','w');
fwrite(fileID,data3,'*int16');
fclose(fileID);

ch1=int16(0*sample*gain);
ch2=ch1;
ch3=ch1;
ch4=int16(post*sample*gain);

data4=[ch1; ch2; ch3; ch4;];

fileID = fopen('chirpchannel4.bin','w');
fwrite(fileID,data4,'*int16');
fclose(fileID);

ch1=int16(0*sample*gain);
ch2=ch1;
ch3=ch1;
ch4=ch1;

data5=[ch1; ch2; ch3; ch4;];

fileID = fopen('zeros.bin','w');
fwrite(fileID,data5,'*int16');
fclose(fileID);
```

createTRIR_averages.m

```
% creates TRIR from chirp responses. Uses the appropriate amount of
% averages
close all; clear;

IRlength = 262144; % set equal to mem
%% extract and save data

N=1; %number of loudspeakers

M=1; %number of averages

trir = zeros(N,IRlength);
for n=1:N

    filename = ['chirpresp',num2str(n)];
    file = dlmread(filename,'\t',4,1);
    chirpresp = file(:,1);

    % Averaging Part

    temp=zeros(IRlength,M);
    for m=1:M
        temp(:,m)=chirpresp((m-1)*IRlength+1:m*IRlength);
    end
    chirpresp = sum(temp,2)/M;

    [chirpsig,FS] = audioread('chirp.wav');

    [IR,b] = impresp(chirpsig,chirpresp);
    save('IR.mat','IR')

    trir(n,:) = 100/max(abs(b'))*b'; % normalizes trir to 100
    n/N*100 % percent done
end

post=1; %maybe wrong name

if N == 1
    data1=[int16(post*trir(1,:)) int16(zeros(length(trir(1,:)),1))'];
    data1=[data1 int16(zeros(6*length(trir(1,:)),1))']; %fills the rest of
the signal with zeros
elseif N == 2
    data1=[int16(post*trir(1,:)) int16(zeros(length(trir(1,:)),1))'
int16(post*trir(2,:)) int16(zeros(length(trir(1,:)),1))'];
    data1=[data1 int16(zeros(4*length(trir(1,:)),1))'];
elseif N == 3
    data1=[int16(post*trir(1,:)) int16(zeros(length(trir(1,:)),1))'
int16(post*trir(2,:)) int16(zeros(length(trir(1,:)),1))'
int16(post*trir(3,:)) int16(zeros(length(trir(1,:)),1))'];
    data1=[data1 int16(zeros(2*length(trir(1,:)),1))'];
elseif N == 4
    data1=[int16(post*trir(1,:)) int16(zeros(length(trir(1,:)),1))'
int16(post*trir(2,:)) int16(zeros(length(trir(1,:)),1))'
```

```
int16(post*trir(3,:)) int16(zeros(length(trir(1,:)),1))'
int16(post*trir(4,:)) int16(zeros(length(trir(1,:)),1))'];
elseif N == 5
    data1=[int16(post*trir(1,:)) int16(zeros(length(trir(1,:)),1))'
int16(post*trir(2,:)) int16(zeros(length(trir(1,:)),1))'
int16(post*trir(3,:)) int16(zeros(length(trir(1,:)),1))'
int16(post*trir(4,:)) int16(zeros(length(trir(1,:)),1))'];
    data2=[int16(post*trir(5,:)) int16(zeros(length(trir(1,:)),1))'];
    data2=[data2 int16(zeros(6*length(trir(1,:)),1))']; %fills the rest of
the signal with zeros
elseif N == 6
    data1=[int16(post*trir(1,:)) int16(zeros(length(trir(1,:)),1))'
int16(post*trir(2,:)) int16(zeros(length(trir(1,:)),1))'
int16(post*trir(3,:)) int16(zeros(length(trir(1,:)),1))'
int16(post*trir(4,:)) int16(zeros(length(trir(1,:)),1))'];
    data2=[int16(post*trir(5,:)) int16(zeros(length(trir(1,:)),1))'
int16(post*trir(6,:)) int16(zeros(length(trir(1,:)),1))'];
    data2=[data2 int16(zeros(4*length(trir(1,:)),1))'];
elseif N == 7
    data1=[int16(post*trir(1,:)) int16(zeros(length(trir(1,:)),1))'
int16(post*trir(2,:)) int16(zeros(length(trir(1,:)),1))'
int16(post*trir(3,:)) int16(zeros(length(trir(1,:)),1))'
int16(post*trir(4,:)) int16(zeros(length(trir(1,:)),1))'];
    data2=[int16(post*trir(5,:)) int16(zeros(length(trir(1,:)),1))'
int16(post*trir(6,:)) int16(zeros(length(trir(1,:)),1))'
int16(post*trir(7,:)) int16(zeros(length(trir(1,:)),1))'];
    data2=[data2 int16(zeros(2*length(trir(1,:)),1))'];
elseif N == 8
    data1=[int16(post*trir(1,:)) int16(zeros(length(trir(1,:)),1))'
int16(post*trir(2,:)) int16(zeros(length(trir(1,:)),1))'
int16(post*trir(3,:)) int16(zeros(length(trir(1,:)),1))'
int16(post*trir(4,:)) int16(zeros(length(trir(1,:)),1))'];
    data2=[int16(post*trir(5,:)) int16(zeros(length(trir(1,:)),1))'
int16(post*trir(6,:)) int16(zeros(length(trir(1,:)),1))'
int16(post*trir(7,:)) int16(zeros(length(trir(1,:)),1))'
int16(post*trir(8,:)) int16(zeros(length(trir(1,:)),1))'];
elseif N > 8
    display('Too many speakers')
end

newmem = 2*IRlength

gain = 4000/max(abs(data1));% scale to 4000
data1 = gain*data1;

fileID = fopen('TRIR1.bin','w'); % creates output for card 1
fwrite(fileID,data1,'*int16');
fclose(fileID);

if N > 4
    gain = 4000/max(abs(data2));% scale to 4000
    data2 = gain*data2;
    fileID = fopen('TRIR2.bin','w'); % creates output for card 2
    fwrite(fileID,data2,'*int16');
    fclose(fileID);
```

```
end
```

savefocus_averages.m

```
% close all; clear;
Focuslength = 1048576;

filename='focus';
file=dlmread(filename,'\t',4,1);
resp=file(:,1);

% averaging

M = 5; %number of averages

temp=zeros(Focuslength,M);
for m=1:M
    temp(:,m)=resp((m-1)*Focuslength+1:m*Focuslength);
end
resp = sum(temp,2)/M;

FS=50000;

%% zero mean
ampl = max(abs(resp))

DCoff2 = mean(resp);

resp = resp - DCoff2;

away=resp;

% ampl = max(abs(resp))
%% Save file

% audiowrite([filename ,'.wav'],resp/(max(abs(resp))),FS); % reduces gain to
avoid clipping
fileID = fopen('focus.bin','w');
fwrite(fileID,resp,'*int16');
fclose(fileID);

save('focus.mat','resp')

%% plot
figure
hold on
plot(resp)
title(['Signal ' filename])
```

SpectrumExample.vi Block Diagram Explanation

As seen in Fig. B.2, the LabVIEW code mainly consists of a while loop and a case structure with 10 cases.

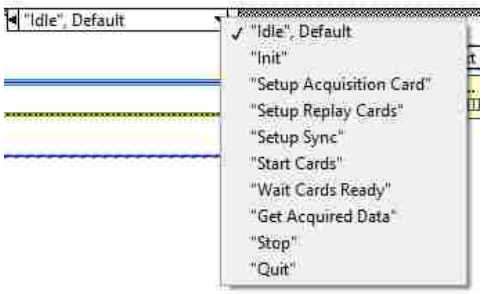

FIG. B. 2 Case structure cases.

The while loop continues iterating until the .vi is quit. Each of the 10 cases follows a logical step in the data acquisition process. A brief description of each case is outlined below.

1. Idle: The condition of the .vi while waiting for a command.
2. Init: Determines the status of the cards.
3. Setup Acquisition Card: Inputs the acquisition parameters defined by the user.
4. Setup Replay Cards: Inputs the generation parameters defined by the user and loads in the user-defined signal. There are two tabs in the stacked sequence structure, one for the first generator card and the other for the second. Below are four key steps in this case (see Fig. B.3).
    a. The .vi reads in the user named data file.

b. The file is separated into four different signals and are ready to be sent to the generator card.

c. The signals are read into the generator card.

d. The signals are plotted.

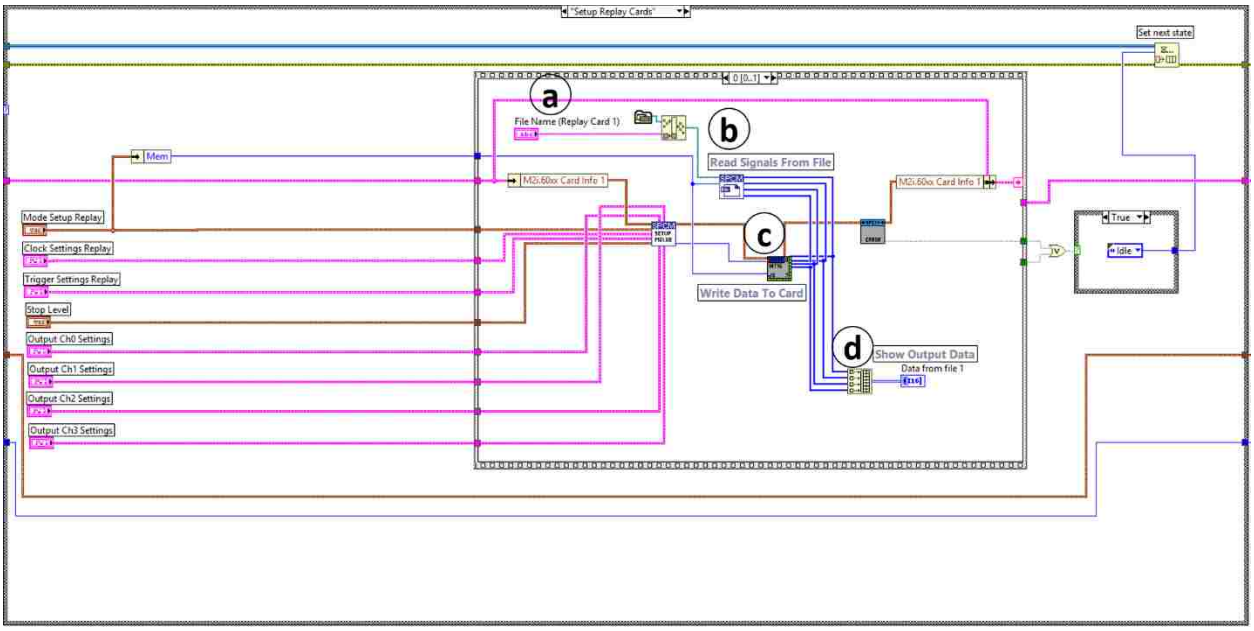

FIG. B.3. SpectrumExample.vi setup replay cards.

5. Setup Sync: Allows for synchronous generation and acquisition.
6. Start Cards: Checks for errors before starting generator cards.
7. Wait Cards Ready: Final check before starting both generation and acquisition.
8. Get Acquired Data: The digitizer card reads in data from the four input channels and they are plotted and saved (see Fig. B.4.)

    a. Data from the digitizer card.

    b. Data is sent to save options and is saved depending on the user input.

c. Data is plotted.

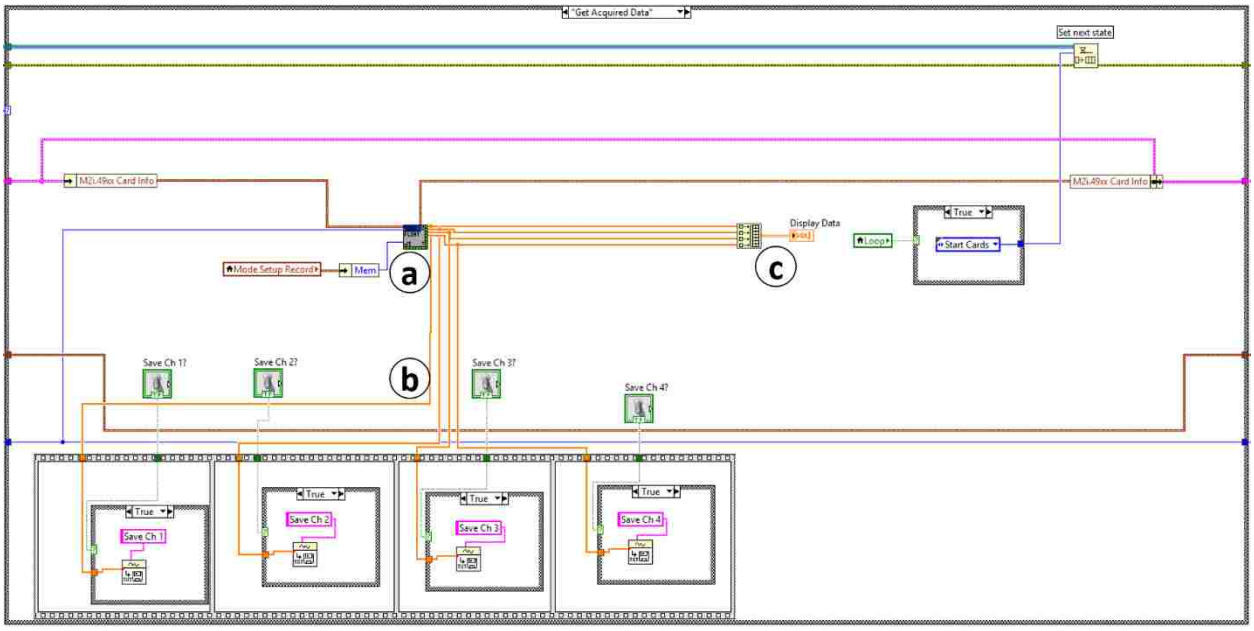

FIG. B.4. Data paths in Get Acquired Data

9. Stop: Stops the current generator/acquisition iteration and resets the .vi.
10. Quit: Allows the .vi to quit.

Figures B.3 and B.4 are shown to help future researchers understand where the raw data is in SpectrumExample.vi. Manipulation in the forward step, including deconvolution, one-bit, clipping, and decay compensation signal processing strategies, can be incorporated in the window shown by Fig. B.3. Additional processing of the focal signal could be included in the window shown by Fig. B.4.